

Multi-configuration time-dependent density-functional theory based on range separation

Emmanuel Fromager^a, Stefan Knecht^b and Hans Jørgen Aa. Jensen^b

*^aLaboratoire de Chimie Quantique,
Institut de Chimie,
CNRS / Université de Strasbourg,
4 rue Blaise Pascal,
67000 Strasbourg, France.*

*^bDepartment of Physics,
Chemistry and Pharmacy,
University of Southern Denmark,
Campusvej 55,
DK-5230 Odense M, Denmark.*

arXiv:1211.4829v2 [physics.chem-ph] 14 Jan 2013

Abstract

Multi-configuration range-separated density-functional theory is extended to the time-dependent regime. An exact variational formulation is derived. The approximation, which consists in combining a long-range *Multi-Configuration-Self-Consistent Field* (MCSCF) treatment with an adiabatic short-range density-functional (DFT) description, is then considered. The resulting time-dependent multi-configuration short-range DFT (TD-MC-srDFT) model is applied to the calculation of singlet excitation energies in H₂, Be and ferrocene, considering both short-range local density (srLDA) and generalized gradient (srGGA) approximations. In contrast to regular TD-DFT, TD-MC-srDFT can describe double excitations. As expected, when modeling long-range interactions with the MCSCF model instead of the adiabatic Buijse-Baerends density-matrix functional as recently proposed by Pernal [K. Pernal, J. Chem. Phys. **136**, 184105 (2012)], the description of both the 1^1D doubly-excited state in Be and the $1^1\Sigma_u^+$ state in the stretched H₂ molecule are improved, although the latter is still significantly underestimated. Exploratory TD-MC-srDFT/GGA calculations for ferrocene yield in general excitation energies at least as good as TD-DFT/CAM-B3LYP, and superior to wave-function (TD-MCSCF, symmetry adapted cluster-configuration interaction) and TD-DFT results based on LDA, GGA, and hybrid functionals.

I. INTRODUCTION

Time-dependent density-functional theory (TD-DFT) [1, 2] is used routinely nowadays for computing electronic excitation energies and transition properties of molecules and solids. Even though low-lying excitation energies often can be obtained sufficiently accurate at a relatively low computational cost, adiabatic TD-DFT using pure functionals usually fails in describing, for example, charge transfers and double excitations. While charge transfers often can be modeled adequately with range-separated hybrid functionals [3–7], where the long-/short-range decomposition of the electron-electron repulsion is used only for the exchange energy, the double excitations remain problematic for all standard exchange-correlation functionals as long as the adiabatic approximation is used for the time-dependent exchange and correlation density-functional [8–11]. This statement holds for hybrid functionals even though non-adiabatic effects can be taken into account through the exact exchange functional, due to the fact that the Kohn-Sham (KS) orbitals are non-local (in time) functionals of the density [12–14]. The accurate description of charge-transfer states in molecular complexes is of particular interest because of their prominent role in for example organic electronics [15] and dye-sensitized solar cell applications [16]. To this end, more sophisticated functionals such as LRC-BOP [5, 17], CAM-B3LYP [18], as well as LC- ω -PBE [19] and other types of range-separated hybrids have been developed [20–22].

In order to further improve standard TD-DFT, in particular for the description of double excitations, Pernal [23] recently proposed to combine it with time-dependent density-matrix functional theory (TD-DMFT) by means of range separation. While describing the long-range part of the electron-electron interaction with the Buijse-Baerends (BB) density-matrix functional, the short-range interaction is treated within the local density approximation (srLDA), both within the adiabatic approximation. The author has tested on H₂ and Be, and she found that the combined method performs much better than standard TD-LDA and TD-DMFT-BB for many excitations, provided the range separation parameter is properly chosen. However, large errors were obtained for the 1^1D double excitation in Be as well as for the $1^1\Sigma_u^+$ state in the stretched H₂ molecule. As an alternative to the long-range adiabatic TD-DMFT-BB treatment, we propose in this work to describe the long-range interaction at the time-dependent *Multi-Configuration Self-Consistent Field* (TD-MCSCF) level, extending thus the MC-srDFT [24] model to the time-dependent regime.

The paper is organized as follows: after a short introduction to time-independent range-separated DFT (Sec. II A), an exact and variational time-dependent formulation is presented in Sec. II B. The approximate linear response TD-MC-srDFT scheme, which consists in describing the long-range interaction at the TD-MCSCF level and the short-range interaction within adiabatic TD-DFT, is then introduced and discussed in Secs. II C and II D. The new scheme is applied to two widely varied types of atomic and molecular systems. We first study the paradigm systems H_2 and Be to illustrate fundamental benefits of the TD-MC-srDFT approach by comparing to other suggestions for how to go beyond Kohn-Sham DFT. We further demonstrate the performance of the new TD-MC-srDFT scheme in an investigation of the low-lying singlet excitations of ferrocene. Thus, following the computational details (Sec. III), numerical results obtained for singlet excitations in H_2 (Secs. IV A and IV B), Be (Sec. IV C) are discussed. In Sec. IV D we elaborate on valence- and charge-transfer singlet excitations in the transition-metal compound ferrocene before drawing conclusions in Sec. V.

II. THEORY

This section deals with the rigorous formulation of variational range-separated TD-DFT models where the range separation is used for both exchange and correlation energies. Introducing first range-separated DFT in Sec. II A, its extension to the time-dependent regime is then presented in Sec. II B. In particular, the derivation of an exact variational formulation is detailed, in the light of Vignale’s recent work [25, 26] on the Runge and Gross variational principle in TD-DFT. For practical calculations, an adiabatic variational formulation is also given. The approximate TD-MC-srDFT model, where the long-range interaction is described within the TD-MCSCF approach, is then derived in Sec. II C using Floquet theory. The interpretation of the TD-MC-srDFT poles as excitation energies is then discussed in Sec. II D.

The theory in this section is completely general in the sense that it is valid for any reasonable range-separation of the two-electron repulsion, however, we will for simplicity describe the theory with the most commonly used choice for the range-separation:

$$\begin{aligned}
 w_{ee}^{\text{lr},\mu}(r_{12}) &= \text{erf}(\mu r_{12})/r_{12}, \\
 w_{ee}^{\text{sr},\mu}(r_{12}) &= \text{erfc}(\mu r_{12})/r_{12} = 1/r_{12} - w_{ee}^{\text{lr},\mu}(r_{12}),
 \end{aligned}
 \tag{1}$$

which depends on the parameter μ . We note that with this choice one has a continuous class of different range-separations when varying μ from zero to infinity: in the $\mu = 0$ limit the long-range part is zero, $w_{ee}^{\text{lr},0}(r_{12}) = 0$, while in the $\mu = +\infty$ limit the short-range part is zero, $w_{ee}^{\text{sr},+\infty}(r_{12}) = 0$.

A. Range-separated density-functional theory

In multi-determinant range-separated DFT, which in the remainder of this paper is simply referred to as short-range DFT (srDFT), the exact ground-state energy of an electronic system can be expressed as

$$E = \min_{\Psi} \left\{ \langle \Psi | \hat{T} + \hat{W}_{ee}^{\text{lr},\mu} + \hat{V}_{\text{ne}} | \Psi \rangle + E_{\text{Hxc}}^{\text{sr},\mu}[n_{\Psi}] \right\}, \quad (2)$$

where \hat{T} is the kinetic energy operator, $\hat{W}_{ee}^{\text{lr},\mu}$ denotes the long-range two-electron interaction, \hat{V}_{ne} is the nuclear potential operator, and $E_{\text{Hxc}}^{\text{sr},\mu}[n]$ denotes the μ -dependent short-range Hartree-exchange-correlation (srHxc) density-functional which describes the complementary short-range energy [27, 28]. The minimizing wave function Ψ^{μ} in Eq. (2) fulfills the following self-consistent equation:

$$\left(\hat{T} + \hat{W}_{ee}^{\text{lr},\mu} + \hat{V}_{\text{ne}} + \hat{V}_{\text{Hxc}}^{\text{sr},\mu}[n_{\Psi^{\mu}}] \right) |\Psi^{\mu}\rangle = \mathcal{E}^{\mu} |\Psi^{\mu}\rangle, \quad (3)$$

$$\hat{V}_{\text{Hxc}}^{\text{sr},\mu}[n] = \int d\mathbf{r} \frac{\delta E_{\text{Hxc}}^{\text{sr},\mu}}{\delta n(\mathbf{r})}[n] \hat{n}(\mathbf{r}),$$

where $\hat{n}(\mathbf{r})$ is the density operator. It is readily seen from Eqs. (2) and (3) that srDFT reduces to standard Kohn-Sham (KS) DFT and pure wave function theory (WFT) in the $\mu = 0$ and $\mu \rightarrow +\infty$ limits, respectively. A combined WFT-srDFT approach is then obtained for intermediate μ values. The approximate Hartree-Fock-srDFT (HF-srDFT) scheme consists in restricting the minimization in Eq. (2) over single-determinant wave functions. It is very similar to range-separated hybrid schemes where the range separation is only used for the exchange energy [4–7]. The two approaches differ by the fact that HF-srDFT does not describe long-range correlation effects since, in srDFT, the range separation is also used for the correlation energy. In the case of multi-configurational systems, the minimization in Eq. (2) should be performed over MCSCF-type wave functions instead. This scheme is referred to as MC-srDFT [24, 29] in the following. Note that correlated methods such

as second-order Møller-Plesset perturbation theory (MP2) [30], Random-Phase Approximation (RPA) [31, 32], Coupled-Cluster (CC) [33] and second-order n -electron valence state perturbation theory (NEVPT2) [34] have also been applied in this context, using the non-variational formulation of srDFT which is given in Eq. (3). It is important to mention that, when describing the long-range interaction at the post-HF level and the short-range interaction with a short-range density-functional, there is no risk of double counting electron correlation effects, which is essential for a combined post-HF-DFT approach. In this respect, using a range-separation of the two-electron repulsion is very appealing. On the other hand, the performance of post-HF-srDFT models will depend on how correlation effects can be split into long- and short-range contributions. This is clear in van der Waals systems in which, for example, MP2-srDFT or CC-srDFT models perform relatively well [30, 33]. In multi-configurational systems, however, it is in general not possible to interpret static and dynamical correlations as long- and short-range ones, respectively. As a result, even though MC-srDFT performs better than regular DFT in stretched molecules for example [24], the approximate short-range density-functional part of the energy is usually not accurate enough since it has somehow to describe a part of static correlation [35]. In this respect, approximate short-range functionals that have been developed so far (see Sec. III) need improvements and work is currently in progress in this direction.

In this paper, the time-dependent regime will be explored in details only for the variational HF-srDFT and MC-srDFT methods. The extension to non-variational srDFT schemes, which is briefly mentioned in Sec. II B, is left for future work.

B. Variational principle in the time-dependent regime

The extension of exact srDFT to the time-dependent regime could in principle be achieved when considering the time-dependent Schrödinger equation of an auxiliary long-range interacting system [23], according to the first Runge and Gross theorem [1], that is without using a variational principle. If the long-range interaction is treated approximately, at the MC-SCF level for example, the Ehrenfest theorem [36] could then be applied in order to obtain the time-dependent MC-srDFT response functions. As an alternative, we explore in this section the possibility of formulating exact time-dependent srDFT variationally, using the quasienergy formalism [37]. As pointed out in Ref. [38], the latter is arguably more attractive

than the Ehrenfest method in that it provides a unified framework for applying variational and non-variational long-range post-HF methods, by analogy with time-independent theory, to which it naturally reduces in the limit of a static local potential [37]. As an additional advantage, the permutational symmetries (with respect to the exchange of perturbation operators) is manifest in the quasienergy method.

In order to obtain a time-dependent extension of Eq. (2), we use in the following the recent work of Vignale [25, 26]. Let us consider the action integral [1] expression

$$\mathcal{Q}[\Psi] = \int_{t_0}^{t_1} Q[\Psi](t) dt, \quad (4)$$

$$Q[\Psi](t) = \frac{\langle \Psi(t) | \hat{T} + \hat{W}_{ee} + \hat{V}(t) - i \frac{\partial}{\partial t} | \Psi(t) \rangle}{\langle \Psi(t) | \Psi(t) \rangle},$$

which is defined for a given time-dependent wave function $\Psi(t)$ and a given time-dependent local potential $\hat{V}(t) = \int d\mathbf{r} v(\mathbf{r}, t) \hat{n}(\mathbf{r})$. The operator \hat{W}_{ee} denotes the regular two-electron repulsion. Note that, in Eq. (4), $\Psi(t)$ is not assumed to be normalized so that, when considering infinitesimal variations of the time-dependent quasienergy $Q[\Psi](t)$ in the following, no normalization constrain will be needed. For time-independent local potentials and wave functions, the time-dependent quasienergy reduces to the usual energy. In Floquet theory, which is considered in Sec. II C, the action integral over a period T equals what is usually referred to as a *quasienergy* [37, 38] multiplied by T . In the general (non-periodic) case, the quasienergy would be equal to the action integral divided by $(t_1 - t_0)$, which is a constant. For simplicity, we will refer to $\mathcal{Q}[\Psi]$ as quasienergy even though it is an action and not an energy, strictly speaking. The time-dependent Schrödinger equation

$$\left(\hat{T} + \hat{W}_{ee} + \hat{V}(t) - i \frac{\partial}{\partial t} \right) |\tilde{\Psi}(t)\rangle = Q[\tilde{\Psi}](t) |\tilde{\Psi}(t)\rangle, \quad (5)$$

where $|\tilde{\Psi}(t_0)\rangle$ is assumed to be normalized, is then equivalent to the variational principle based on the quasienergy

$$\delta \mathcal{Q}[\tilde{\Psi}] = -i \left[\langle \tilde{\Psi}(t) | \delta \Psi(t) \rangle \right]_{t_0}^{t_1}, \quad (6)$$

where variations $|\tilde{\Psi}(t)\rangle \rightarrow |\tilde{\Psi}(t)\rangle + \delta \Psi(t)$ around the exact solution $|\tilde{\Psi}(t)\rangle$ are considered. Using the boundary conditions $\delta \Psi(t_0) = \delta \Psi(t_1) = 0$, the variational principle can be simply written as

$$\delta \mathcal{Q}[\tilde{\Psi}] = 0. \quad (7)$$

This stationary condition is convenient for deriving approximate time-dependent response properties based on variational methods such as HF and MCSCF [37]. The time-dependent extension of both HF-srDFT and MC-srDFT schemes can then be achieved along the same lines, provided that time-dependent srDFT can be expressed in terms of a variational principle, which is actually not trivial [25, 26]. This point is addressed in the rest of this section. According to the first Runge and Gross theorem [1], for a fixed initial wave function $\tilde{\Psi}(t_0)$, the following density-functional quasienergy can be defined:

$$\mathcal{Q}[n] = \mathcal{B}[n] + \int_{t_0}^{t_1} dt \int d\mathbf{r} v(\mathbf{r}, t)n(\mathbf{r}, t), \quad (8)$$

where the universal functional

$$\mathcal{B}[n] = \int_{t_0}^{t_1} dt \langle \tilde{\Psi}[n](t) | \hat{T} + \hat{W}_{ee} - i \frac{\partial}{\partial t} | \tilde{\Psi}[n](t) \rangle, \quad (9)$$

is calculated with the time-dependent wave function $\tilde{\Psi}[n](t)$ associated to a fully interacting system whose time-dependent density equals $n(\mathbf{r}, t)$:

$$\left(\hat{T} + \hat{W}_{ee} + \hat{V}[n](t) - i \frac{\partial}{\partial t} \right) | \tilde{\Psi}[n](t) \rangle = Q[n](t) | \tilde{\Psi}[n](t) \rangle, \quad (10)$$

$$\hat{V}[n](t) = \int d\mathbf{r} v[n](\mathbf{r}, t) \hat{n}(\mathbf{r}).$$

The density $\tilde{n}(\mathbf{r}, t)$ associated to the exact solution $\tilde{\Psi}(t)$ of the time-dependent Schrödinger Eq. (5) can then be obtained when applying the following variational principle

$$\delta \mathcal{Q}[\tilde{n}] = -i \langle \tilde{\Psi}[\tilde{n}](t_1) | \delta \tilde{\Psi}[\tilde{n}](t_1) \rangle, \quad (11)$$

where the boundary condition $\delta \tilde{\Psi}[\tilde{n}](t_0) = 0$ was used. As pointed out by Vignale [25], though the boundary conditions $\delta n(\mathbf{r}, t_0) = \delta n(\mathbf{r}, t_1) = 0$ are fulfilled, the condition $\delta \mathcal{Q}[\tilde{n}] = 0$ is *not*. Indeed, the wave function $\tilde{\Psi}[\tilde{n} + \delta n](t) = \tilde{\Psi}[\tilde{n}](t) + \delta \tilde{\Psi}[\tilde{n}](t)$ accumulates the change of the density $\delta n(\mathbf{r}, t)$ over the time interval $[t_0, t_1]$:

$$\begin{aligned} \delta \tilde{\Psi}[\tilde{n}](t_1) &= \int_{t_0}^{t_1} dt \int d\mathbf{r} \frac{\delta \tilde{\Psi}}{\delta n(\mathbf{r}, t)}[\tilde{n}](t_1) \delta n(\mathbf{r}, t) \\ &\neq 0, \end{aligned} \quad (12)$$

so that the variational principle in Eq. (11) can be rewritten as

$$\frac{\delta \mathcal{Q}}{\delta n(\mathbf{r}, t)}[\tilde{n}] = -i \left\langle \tilde{\Psi}[\tilde{n}](t_1) \left| \frac{\delta \tilde{\Psi}}{\delta n(\mathbf{r}, t)}[\tilde{n}](t_1) \right. \right\rangle. \quad (13)$$

As in the time-independent regime (see Sec. II A), the universal functional $\mathcal{B}[n]$ defined in Eq. (9) can be split into long-range and short-range parts:

$$\begin{aligned}\mathcal{B}[n] &= \mathcal{B}^{\text{lr},\mu}[n] + \mathcal{Q}_{\text{Hxc}}^{\text{sr},\mu}[n], \\ \mathcal{B}^{\text{lr},\mu}[n] &= \\ &\int_{t_0}^{t_1} dt \langle \tilde{\Psi}^\mu[n](t) | \hat{T} + \hat{W}_{ee}^{\text{lr},\mu} - i \frac{\partial}{\partial t} | \tilde{\Psi}^\mu[n](t) \rangle,\end{aligned}\tag{14}$$

where $\tilde{\Psi}^\mu[n](t)$ is the time-dependent wave function associated to a long-range interacting system whose density equals $n(\mathbf{r}, t)$:

$$\begin{aligned}&\left(\hat{T} + \hat{W}_{ee}^{\text{lr},\mu} + \hat{V}^\mu[n](t) - i \frac{\partial}{\partial t} \right) | \tilde{\Psi}^\mu[n](t) \rangle \\ &= Q^\mu[n](t) | \tilde{\Psi}^\mu[n](t) \rangle, \\ \hat{V}^\mu[n](t) &= \int d\mathbf{r} v^\mu[n](\mathbf{r}, t) \hat{n}(\mathbf{r}).\end{aligned}\tag{15}$$

Note that the initial state $\tilde{\Psi}^\mu[n](t_0)$ is fixed and equal to the auxiliary long-range interacting wave function $\tilde{\Psi}^\mu(t_0)$ whose density equals the one of the real fully interacting initial wave function $\tilde{\Psi}(t_0)$. The universal long-range functional defined in Eq. (14) can be expressed in terms of the auxiliary long-range interacting time-dependent quasienergy as follows

$$\begin{aligned}\mathcal{B}^{\text{lr},\mu}[n] &= \int_{t_0}^{t_1} dt \left(Q^\mu[n](t) \right. \\ &\quad \left. - \int d\mathbf{r} v^\mu[n](\mathbf{r}, t) n(\mathbf{r}, t) \right),\end{aligned}\tag{16}$$

so that, using the simplified expression

$$\begin{aligned}\int_{t_0}^{t_1} dt \delta Q^\mu[n](t) &= -i \langle \tilde{\Psi}^\mu[n](t_1) | \delta \tilde{\Psi}^\mu[n](t_1) \rangle \\ &+ \int_{t_0}^{t_1} dt \int d\mathbf{r} \delta v^\mu[n](\mathbf{r}, t) n(\mathbf{r}, t),\end{aligned}\tag{17}$$

as well as Eqs. (8) and (14), the variational principle in Eq. (13) provides the exact expression for the local potential which reproduces the time-dependent density $\tilde{n}(\mathbf{r}, t)$ of the fully

interacting wave function $\tilde{\Psi}(t)$ from a long-range interacting one:

$$\begin{aligned}
v^\mu[\tilde{n}](\mathbf{r}, t) &= v(\mathbf{r}, t) + \frac{\delta \mathcal{Q}_{\text{Hxc}}^{\text{sr}, \mu}}{\delta n(\mathbf{r}, t)}[\tilde{n}] \\
&\quad - i \left\langle \tilde{\Psi}^\mu[\tilde{n}](t_1) \left| \frac{\delta \tilde{\Psi}^\mu}{\delta n(\mathbf{r}, t)}[\tilde{n}](t_1) \right. \right\rangle \\
&\quad + i \left\langle \tilde{\Psi}[\tilde{n}](t_1) \left| \frac{\delta \tilde{\Psi}}{\delta n(\mathbf{r}, t)}[\tilde{n}](t_1) \right. \right\rangle.
\end{aligned} \tag{18}$$

It is important to keep in mind that, as further discussed in Sec. IID, the time evolution of the auxiliary long-range interacting system yields the time-dependent response of the *exact* density but *not* the response of the exact wave function. In the particular case of a periodic perturbation, which is considered in the rest of this work, both fully and long-range interacting wave functions remain unchanged after a period T :

$$\tilde{\Psi}[n](t_0 + T) = \tilde{\Psi}[n](t_0) = \tilde{\Psi}(t_0), \tag{19}$$

$$\tilde{\Psi}^\mu[n](t_0 + T) = \tilde{\Psi}^\mu[n](t_0) = \tilde{\Psi}^\mu(t_0),$$

so that, for $t_1 = t_0 + T$, the last two terms in the right-hand side of Eq. (18) are equal to zero. In addition, if the adiabatic approximation is used for describing the short-range interaction, the srHxc density-functional quasienergy expression is simplified as follows:

$$\mathcal{Q}_{\text{Hxc}}^{\text{sr}, \mu}[n] \rightarrow \int_{t_0}^{t_1} dt E_{\text{Hxc}}^{\text{sr}, \mu}[n(t)], \tag{20}$$

where $E_{\text{Hxc}}^{\text{sr}, \mu}[n]$ is the time-independent srHxc density-functional introduced in Eq. (2), and the time-dependent potential in Eq. (18) becomes

$$v^\mu[\tilde{n}](\mathbf{r}, t) \rightarrow v(\mathbf{r}, t) + \frac{\delta E_{\text{Hxc}}^{\text{sr}, \mu}}{\delta n(\mathbf{r})}[\tilde{n}(t)]. \tag{21}$$

Combining Eqs. (3), (15) and (21), we conclude that the time-dependent density $\tilde{n}(\mathbf{r}, t)$ of the real fully interacting system can be approximated from an auxiliary long-range interacting one whose wave function $\tilde{\Psi}^\mu(t)$ fulfills, within the short-range adiabatic approximation,

$$\begin{aligned}
&\left(\hat{T} + \hat{W}_{ee}^{\text{lr}, \mu} + \hat{V}(t) + \hat{V}_{\text{Hxc}}^{\text{sr}, \mu}[n_{\tilde{\Psi}^\mu(t)}] - i \frac{\partial}{\partial t} \right) |\tilde{\Psi}^\mu(t)\rangle \\
&= Q^\mu(t) |\tilde{\Psi}^\mu(t)\rangle,
\end{aligned} \tag{22}$$

which is equivalent to the stationary condition

$$\delta \mathcal{Q}^\mu[\tilde{\Psi}^\mu] = 0, \quad (23)$$

where the wave-function-dependent range-separated quasienergy $\mathcal{Q}^\mu[\Psi]$ is defined as

$$\begin{aligned} \mathcal{Q}^\mu[\Psi] = & \int_{t_0}^{t_1} dt \frac{\langle \Psi(t) | \hat{T} + \hat{W}_{ee}^{\text{lr},\mu} + \hat{V}(t) - i \frac{\partial}{\partial t} | \Psi(t) \rangle}{\langle \Psi(t) | \Psi(t) \rangle} \\ & + \int_{t_0}^{t_1} dt E_{\text{Hxc}}^{\text{sr},\mu}[n_{\Psi(t)}]. \end{aligned} \quad (24)$$

Note that the time-dependent KS equation, as formulated within the adiabatic approximation, is recovered from Eq. (22) when $\mu = 0$, while the $\mu \rightarrow +\infty$ limit corresponds to the time-dependent Schrödinger equation. When $0 < \mu < +\infty$, a rigorous combination of density-functional and wave function theories is obtained in the time-dependent regime. As shown in the following, a multi-configuration extension of regular TD-DFT can then be formulated in this context when describing the long-range interaction at the MCSCF level. Let us mention that non-variational methods such as CC could also be merged with TD-DFT, using Eq. (22) in combination with a Lagrangian formalism [37].

C. Multi-configuration range-separated TD-DFT based on Floquet theory

We work in this section in the framework of Floquet theory [37] where the time-dependent perturbation is periodic:

$$\begin{aligned} \hat{V}(t) = & \hat{V}_{\text{ne}} + \sum_x \sum_{k=-N}^N e^{-i\omega_k t} \varepsilon_x(\omega_k) \hat{V}_x, \\ \omega_k = & \frac{2\pi k}{T}, \end{aligned} \quad (25)$$

$$\hat{V}_x = \int d\mathbf{r} v_x(\mathbf{r}) \hat{n}(\mathbf{r}),$$

and the quasienergy in Eq. (24) is calculated over a period $\int_{t_0}^{t_1} dt \rightarrow \int_0^T dt$. Since the long-range interaction in Eq. (22) is treated explicitly, the exact time-dependent wave function $\tilde{\Psi}^\mu(t)$ is a multi-determinant one. As an approximation, we consider the following MCSCF-type parametrization consisting of exponential unitary transformations [36]:

$$|\tilde{\Psi}^\mu(t)\rangle = e^{i\hat{\kappa}(t)} e^{i\hat{S}(t)} |\Psi_0^\mu\rangle, \quad (26)$$

where Ψ_0^μ denotes the unperturbed time-independent MC-srDFT wave function and

$$\hat{\kappa}(t) = \sum_{l,i} e^{-i\omega_l t} \kappa_i(\omega_l) \hat{q}_i^\dagger + e^{-i\omega_l t} \kappa_i^*(-\omega_l) \hat{q}_i, \quad (27)$$

$$\hat{S}(t) = \sum_{l,i} e^{-i\omega_l t} S_i(\omega_l) \hat{R}_i^\dagger + e^{-i\omega_l t} S_i^*(-\omega_l) \hat{R}_i.$$

The singlet excitation and state-transfer operators are defined as follows

$$\hat{q}_i^\dagger = \hat{E}_{pq} = \hat{a}_{p\alpha}^\dagger \hat{a}_{q\alpha} + \hat{a}_{p\beta}^\dagger \hat{a}_{q\beta}; \quad p > q, \quad (28)$$

$$\hat{R}_i^\dagger = |i\rangle \langle \Psi_0^\mu|.$$

Note that the TD-HF-srDFT scheme is a particular case of Eq. (26), where the unperturbed MC-srDFT wave function would be replaced by the HF-srDFT determinant, and orbital rotations only would be considered. The resulting linear response equations would then be formally identical to standard TD-DFT equations based on hybrid density-functionals [39]. Returning to the multi-configuration case, the TD-MC-srDFT wave function in Eq. (26) is fully determined by the Fourier component vectors

$$\Lambda(\omega_l) = \begin{bmatrix} \kappa_i(\omega_l) \\ S_i(\omega_l) \\ \kappa_i^*(-\omega_l) \\ S_i^*(-\omega_l) \end{bmatrix}, \quad (29)$$

for which we consider in the following the Taylor expansion through first order:

$$\Lambda(\omega_l) = \sum_{k=-N,x}^N \varepsilon_x(\omega_k) \left. \frac{\partial \Lambda(\omega_l)}{\partial \varepsilon_x(\omega_k)} \right|_0 + \dots \quad (30)$$

Rewriting the variational condition in Eq. (23) as follows

$$\forall \varepsilon_x(\omega_k) \quad \frac{\partial \mathcal{Q}^\mu}{\partial \Lambda^\dagger(-\omega_l)} = 0, \quad (31)$$

the linear response equations are simply obtained by differentiation with respect to the perturbation strength $\varepsilon_x(\omega_k)$ [39, 40]:

$$\left(\frac{d}{d\varepsilon_x(\omega_k)} \frac{\partial \mathcal{Q}^\mu}{\partial \Lambda^\dagger(-\omega_l)} \right) \Big|_0 = 0. \quad (32)$$

According to Eq. (24), the quasienergy can be decomposed as follows:

$$\mathcal{Q}^\mu = \mathcal{Q}^{\text{lr},\mu} + \mathcal{Q}_{\text{Hxc}}^{\text{sr},\mu}, \quad (33)$$

where the purely long-range MCSCF part equals

$$\begin{aligned} \mathcal{Q}^{\text{lr},\mu} = & \int_0^T dt \langle \tilde{\Psi}^\mu(t) | \hat{T} + \hat{W}_{ee}^{\text{lr},\mu} + \hat{V}(t) | \tilde{\Psi}^\mu(t) \rangle \\ & + \int_0^T dt \langle \tilde{\Psi}^\mu(t) | -i \frac{\partial}{\partial t} | \tilde{\Psi}^\mu(t) \rangle, \end{aligned} \quad (34)$$

and the purely short-range DFT contribution is written as

$$\mathcal{Q}^{\text{sr},\mu} = \int_0^T E_{\text{Hxc}}^{\text{sr},\mu}[n_{\tilde{\Psi}^\mu(t)}] dt, \quad (35)$$

$$n_{\tilde{\Psi}^\mu(t)}(\mathbf{r}) = \langle \tilde{\Psi}^\mu(t) | \hat{n}(\mathbf{r}) | \tilde{\Psi}^\mu(t) \rangle.$$

The terms arising from the derivatives of the former can be computed with a regular linear response MCSCF code [36, 41], using long-range two-electron integrals, and thus do not require additional implementation efforts. On the other hand, standard TD-DFT codes cannot be used straightforwardly for computing the srDFT terms since the density is now obtained from a MCSCF-type wave function instead of a single KS determinant, terms describing how the density changes when the configuration coefficients change are also needed. The srDFT contributions to the linear response equations can be decomposed as follows

$$\begin{aligned} & \left(\frac{d}{d\varepsilon_x(\omega_k)} \frac{\partial \mathcal{Q}^{\text{sr},\mu}}{\partial \Lambda^\dagger(-\omega_l)} \right) \Big|_0 = \frac{d}{d\varepsilon_x(\omega_k)} \frac{\partial}{\partial \Lambda^\dagger(-\omega_l)} \\ & \left(\int_0^T \langle \tilde{\Psi}^\mu(t) | \hat{V}_{\text{Hxc}}^{\text{sr},\mu}[n_{\tilde{\Psi}_0^\mu}] | \tilde{\Psi}^\mu(t) \rangle dt \right. \\ & \left. + \frac{T}{2} \sum_{m,n} \delta(\omega_m + \omega_n) \int d\mathbf{r} d\mathbf{r}' K_{\text{Hxc}}^{\text{sr},\mu}(\mathbf{r}, \mathbf{r}') \right. \\ & \left. \times \Lambda^\dagger(-\omega_m) n^{[1]\mu}(\mathbf{r}) n^{[1]\mu\dagger}(\mathbf{r}') \Lambda(\omega_n) \right) \Big|_0, \end{aligned} \quad (36)$$

where $K_{\text{Hxc}}^{\text{sr},\mu}(\mathbf{r}, \mathbf{r}') = \delta^2 E_{\text{Hxc}}^{\text{sr},\mu} / \delta n(\mathbf{r}) \delta n(\mathbf{r}') [n_{\Psi_0^\mu}]$ denotes the srHxc kernel calculated for the unperturbed density and the gradient density vector equals

$$n^{[1]\mu}(\mathbf{r}) = \begin{bmatrix} \langle \Psi_0^\mu | [\hat{q}_i, \hat{n}(\mathbf{r})] | \Psi_0^\mu \rangle \\ \langle \Psi_0^\mu | [\hat{R}_i, \hat{n}(\mathbf{r})] | \Psi_0^\mu \rangle \\ \langle \Psi_0^\mu | [\hat{q}_i^\dagger, \hat{n}(\mathbf{r})] | \Psi_0^\mu \rangle \\ \langle \Psi_0^\mu | [\hat{R}_i^\dagger, \hat{n}(\mathbf{r})] | \Psi_0^\mu \rangle \end{bmatrix}. \quad (37)$$

The linear response Eq. (32) can thus be rewritten as [36, 41]

$$\left(E^{[2]\mu} - \omega_l S^{[2]\mu} \right) \frac{\partial \Lambda(-\omega_l)}{\partial \varepsilon_x(\omega_k)} \Big|_0 = i V_x^{[1]\mu} \delta(\omega_k + \omega_l), \quad (38)$$

where the Hessian is split as follows:

$$E^{[2]\mu} = E_0^{[2]\mu} + K_{\text{Hxc}}^{\text{sr},\mu}. \quad (39)$$

The MCSCF-type Hessian $E_0^{[2]\mu}$ is based on the auxiliary long-range interacting Hamiltonian $\hat{T} + \hat{W}_{ee}^{\text{lr},\mu} + \hat{V}_{\text{ne}} + \hat{V}_{\text{Hxc}}^{\text{sr},\mu} [n_{\Psi_0^\mu}]$, that is used as H_0 in Eqs. (9) and (10) of Ref. [41], and the srHxc kernel contribution is defined as

$$K_{\text{Hxc}}^{\text{sr},\mu} = \int d\mathbf{r} d\mathbf{r}' K_{\text{Hxc}}^{\text{sr},\mu}(\mathbf{r}, \mathbf{r}') n^{[1]\mu}(\mathbf{r}) n^{[1]\mu\dagger}(\mathbf{r}'). \quad (40)$$

Both $E_0^{[2]\mu}$ and $S^{[2]\mu}$ matrices (see Eqs. (7) and (8) in Ref. [41]) are built from the unperturbed MC-srDFT wave function Ψ_0^μ and the gradient property vector $V_x^{[1]\mu}$ equals $\int d\mathbf{r} v_x(\mathbf{r}) n^{[1]\mu}(\mathbf{r})$. Excitation energies can thus be calculated at the MC-srDFT level when solving iteratively [41]

$$\left(E^{[2]\mu} - \omega S^{[2]\mu} \right) X(\omega) = 0, \quad (41)$$

which can be considered a multi-configuration extension of the Casida equations [2].

D. Interpretation of the TD-MC-srDFT poles

The linear response Eq. (41) computes the poles of the TD-MC-srDFT wave function. As already mentioned in Sec. II B, a solution can only be interpreted as an excitation energy if it is a pole of the TD-MC-srDFT density. In this respect, the double excitation recovered in the $\mu = 0$ limit of a simple two-state TD-MC-srDFT model (see Appendix) is not physical.

It is in principle less problematic for non-zero μ values, even small ones, since the ground-state MC-srDFT wave function becomes multi-determinantal. This is analyzed further in Secs. IV B and IV C. In order to obtain a smoother connection to regular TD-DFT when $\mu \rightarrow 0$, an effective orbital rotation vector

$$\tilde{\mathcal{K}}(\omega_l) = \begin{bmatrix} \tilde{\kappa}_i(\omega_l) \\ \tilde{\kappa}_i^*(-\omega_l) \end{bmatrix}, \quad (42)$$

such that

$$\begin{aligned} \tilde{n}^{[1]\mu\dagger}(\mathbf{r})\tilde{\mathcal{K}}(\omega_l) &= n^{[1]\mu\dagger}(\mathbf{r})\Lambda(\omega_l), \\ \tilde{n}^{[1]\mu\dagger}(\mathbf{r}) &= \begin{bmatrix} \langle \Psi_0^\mu | [\hat{q}_i, \hat{n}(\mathbf{r})] | \Psi_0^\mu \rangle \\ \langle \Psi_0^\mu | [\hat{q}_i^\dagger, \hat{n}(\mathbf{r})] | \Psi_0^\mu \rangle \end{bmatrix}, \end{aligned} \quad (43)$$

could be introduced and the TD-MC-srDFT linear response Eq. (38) reformulated in terms of $\partial\tilde{\mathcal{K}}(-\omega_l)/\partial\varepsilon_x(\omega_k)\Big|_0$. Work is currently in progress in this direction.

III. COMPUTATIONAL DETAILS

The TD-MC-srDFT linear response Eq. (38) has been implemented in a development version of the DALTON2011 program package [42]. Calculations have been performed with spin-independent short-range functionals, considering both local density (srLDA) and generalized gradient (srGGA) approximations. In the former case, we used the srLDA functional of Toulouse, Savin and Flad [3, 43]. We used, as srGGA functional, the Perdew-Burke-Ernzerhof-type (PBE) functional of Goll, Werner and Stoll [33], which is denoted srPBEgws in the following. Basis sets are aug-cc-pVQZ [44] for both H₂ and Be systems. We furthermore performed all-electron TD-MC-srDFT linear response calculations of ferrocene Fe(C₅H₅)₂ (iron *bis*-cyclopentadienyl, FeCp₂) examining excitation energies and oscillator strengths of the lowest singlet excited *d-d* and ligand-to-metal charge transfer states. The geometrical parameters for the eclipsed FeCp₂ conformer (D_{5h} symmetry), compiled in Table S1 in the Supplementary Material [45], were taken from the recent work by Coriani *et al.* [46] who carried out highly accurate geometry optimizations at the CCSD(T) level yielding close agreement with experiment and other available *ab initio* data [47–50]. We employed triple- ζ cc-pVTZ-DK basis sets for all elements [51, 52] where scalar-relativistic effects were

taken into account by means of the Douglas-Kroll-Hess second-order (DKH2) Hamiltonian. We did not account for spin-orbit effects which were found by Scuppa and co-workers [50] to be of only minor importance for the singlet excitation spectrum of ferrocene. The excited state manifold of FeCp_2 was computed with the regular TD-HF and TD-MCSCF approaches as well as the combined TD-HF-srLDA, TD-HF-srPBEgws and TD-MC-srPBEgws models. The initial CASSCF optimization step was performed for both MC-srDFT and regular MCSCF using the well-established CAS(10,10) active space with 10 electrons in 10 orbitals [48], comprising the Cp-ligand π orbitals in addition to the Fe $3d4s$ shells. For analysis purposes, we carried out standard scalar-relativistic DKH2 TD-DFT calculations using pure LDA [53] and PBE [54] functionals, as well as the hybrid Becke three-parameter Lee-Yang-Parr B3LYP [55] and the Coulomb attenuated method CAM-B3LYP [18] functionals, within the adiabatic approximation. The μ parameter was set in all TD-HF-srDFT and TD-MC-srDFT calculations to 0.4 a.u. unless otherwise specified. This value relates to a prescription given in Refs. [24, 56] for an optimal treatment of short-range electron correlation in ground-state MC-srDFT calculations and should, in principle, be re-considered in the time-dependent regime. As illustrated in Sec. IV C, the choice of μ in TD-MC-srDFT calculations is important since it affects excitation energies significantly. This will be further analyzed in future work.

IV. RESULTS AND DISCUSSION

A. ${}^1\Sigma_u^+$ excited states of H_2

Our TD-MC-srDFT calculations have been performed for H_2 with the minimal $1\sigma_g 1\sigma_u$ active space which however can recover ${}^1\Sigma_u^+$ excitation energies very close to the FCI ones already at the TD-MCSCF level (see Fig. 1 (a)). Potential curves obtained with the srLDA and srPBEgws functionals were found to be on top of each other. Therefore only the formers are discussed in the following. As shown in Fig. 1 (b), the TD-HF-srLDA and TD-MC-srLDA methods give, near the equilibrium H-H distance (about 1.4 a.u.), the same excitation energies for the first four ${}^1\Sigma_u^+$ states when μ is set to 0.4 a.u. This is due to the fact that (i) the ground-state HF-srLDA and MC-srLDA wave functions are, in this case, almost identical [24] (ii) these excitations all correspond, predominantly, to single excitations from the $1\sigma_g$ to σ_u

orbitals [57]. The latter are indeed well described by orbital rotations, like in standard TD-DFT, with no need for a long-range multi-configuration treatment. Note that the excitation energies are, in this case, more accurate than the pure TD-LDA ones: using the FCI curves as reference, the error is approximately divided by two. Upon bond stretching, the difference between TD-HF-srLDA and TD-MC-srLDA excitation energies becomes significant for the $4^1\Sigma_u^+$ state already around 2.5 a.u. Indeed, while the former is associated to the singly excited configuration $(1\sigma_g)^1(4\sigma_u)^1$, the latter corresponds to the doubly excited configuration $(1\sigma_u)^1(2\sigma_g)^1$. This double excitation is obtained as a single excitation applied to the doubly excited configuration $(1\sigma_u)^2$ whose weight in the ground-state MC-srLDA wave function is less than 1% but not strictly equal to zero. For the same bond distance, the $3^1\Sigma_u^+$ state, which is dominated by the singly excited configuration $(1\sigma_g)^1(3\sigma_u)^1$, acquires also, but to a less pronounced extent than for $4^1\Sigma_u^+$, a doubly excited character $[(1\sigma_g)^2 \rightarrow (1\sigma_u)^1(2\sigma_g)^1]$. The $1^1\Sigma_u^+$ and $2^1\Sigma_u^+$ states are mainly combinations of the singly excited configurations $(1\sigma_g)^1(1\sigma_u)^1$ and $(1\sigma_g)^1(2\sigma_u)^1$, which explains the smaller difference, compared to the $4^1\Sigma_u^+$ state, between the TD-HF-srLDA and TD-MC-srLDA excitation energies. Around 5 a.u., the $4^1\Sigma_u^+$ state obtained at the TD-MC-srLDA level is dominated by the doubly excited configuration $(1\sigma_u)^1(3\sigma_g)^1$ while, at the regular TD-MCSCF level, both $(1\sigma_u)^1(3\sigma_g)^1$ and $(1\sigma_u)^1(2\sigma_g)^1$ configurations are important. This difference could be justified by the fact that long-range interactions only are described within the MCSCF model while short-range interactions are assigned to DFT. In other words, the ground-state wave function and its linear response are not expected to be the same at the MC-srDFT and regular MCSCF levels. As shown in Sec. II B, this should be expected only for the densities. The large underestimation of the $4^1\Sigma_u^+$ excitation energy, by about 0.1 a.u., is mainly due to the approximate (adiabatic srLDA) potential and kernel used. It is important to notice that the explicit treatment, at the MCSCF level, of the long-range interaction enables a multi-configuration description, within a TD-DFT framework, of the excited states upon bond stretching. This is illustrated by the increasing doubly excited character $[(1\sigma_g)^2 \rightarrow (1\sigma_u)^1(2\sigma_g)^1]$ of the $3^1\Sigma_u^+$ state when enlarging the bond distance from 2.5 to 5 a.u. This explains the increasing difference between the TD-HF-srLDA and TD-MC-srLDA excitation energies. For the latter, the doubly excited character is induced by the single excitation $[(1\sigma_u)^2 \rightarrow (1\sigma_u)^1(2\sigma_g)^1]$ applied, in the long-range MCSCF linear response calculation, to the configuration $(1\sigma_u)^2$ whose weight increases in the ground-state MC-srLDA wave function (0.6% at 2.5 a.u. and

23% at 5 a.u.). Let us mention that, even though TD-HF-srLDA and TD-LDA methods cannot describe double excitations, they provide at 5 a.u. a more accurate $3^1\Sigma_u^+$ excitation energy than the TD-MC-srLDA approach, an example of fortuitous error cancellation. Upon further stretching, both TD-LDA and TD-HF-srLDA potential curves indeed deviate increasingly from the FCI one, while the TD-MC-srLDA curve remains parallel to the latter. Such a fortuitous error cancellation does not happen for the $2^1\Sigma_u^+$ and $1^1\Sigma_u^+$ states, and the TD-MC-srLDA performs better than TD-LDA and TD-HF-srLDA methods upon bond stretching. At 5 a.u., the $2^1\Sigma_u^+$ state is dominated by both singly excited $(1\sigma_g)^1(2\sigma_u)^1$ and doubly excited $(1\sigma_u)^1(2\sigma_g)^1$ configurations for which the MC-srLDA linear response coefficients are equal to 0.33 and 0.13 in absolute value, respectively. On the other hand, the $1^1\Sigma_u^+$ state is dominated by the singly excited $(1\sigma_g)^1(1\sigma_u)^1$ ionic configuration which is included in the active space and thus described, not by orbital rotations, but by configuration rotations instead. As expected [57], the TD-HF-srLDA $1^1\Sigma_u^+$ potential curve does not exhibit a minimum, exactly as with TD-LDA, simply because the $1\sigma_g$ and $1\sigma_u$ orbitals become degenerate in the dissociation limit. On the contrary, the TD-MC-srLDA curve has a minimum. This clearly shows that describing the long-range part of the electron-electron interaction at the MCSCF level in a range-separated TD-DFT framework can improve remarkably the exchange-correlation kernel used in standard TD-DFT calculations. Note also that the TD-DMFT-srLDA ($\mu = 0.7$) $1^1\Sigma_u^+$ excitation energy of Pernal [23] (3.02 eV), which was computed for a bond distance of 10.0 *a.u.*, is largely improved at the TD-MC-srLDA ($\mu = 0.7$) level (8.45 eV) when compared to FCI (9.90 eV). All these results were obtained with the aug-cc-pVTZ [44] basis set. Even though we use a different srLDA functional, we can reasonably conclude that the large errors obtained at the TD-DMFT-srLDA level are essentially due to the long-range adiabatic BB approximation. Returning to the TD-MC-srLDA ($\mu = 0.4$) results, the $1^1\Sigma_u^+$ excitation energy is still significantly underestimated for large bond distances. The srLDA potential and kernel should then be improved in order to obtain more accurate results. One can also notice that the FCI $1^1\Sigma_u^+$ potential curve minimum (around 4 a.u.) is shifted to about 5.5 a.u. at the TD-MC-srLDA level. Indeed, up to bond distances of 4 a.u., there are no significant differences between TD-HF-srLDA and TD-MC-srLDA excitation energies. This is due to the relatively small $\mu = 0.4$ value, which ensures that, at the equilibrium distance, most of the electron correlation is assigned to the short-range interaction and thus treated in DFT. The assignment of static correlation to the

long-range interaction appears clearly in the dissociation limit, that is when both $1\sigma_g$ and $1\sigma_u$ natural orbitals are singly occupied in the ground-state MC-srLDA wave function [24]. For intermediate bond distances, the range-separation of static and dynamic correlations is not clear anymore [35]. It means that the short-range potential and kernel should be accurate enough to obtain reliable excitation energies for distances where a part of static correlation is inevitably assigned to the short-range interaction. The situation is of course less critical for larger μ values but, in this case, more electron correlation must be described by the MCSCF which is not appealing, in terms of computational cost, for larger scale calculations. Using a multi-configuration short-range exact exchange energy expression [58–60] while keeping $\mu = 0.4$ a.u. is a possible alternative currently under investigation. Such a scheme would largely reduce self-interaction errors [24] in the ground-state MC-srLDA energy and is expected to affect excitation energies through the improved short-range potential and kernel.

B. ${}^1\Sigma_g^+$ excited states of H_2

The TD-MC-srLDA method was also applied to the calculation of the first four ${}^1\Sigma_g^+$ states of H_2 , setting μ to 0.4 a.u. and using the minimal $1\sigma_g 1\sigma_u$ active space. The latter enables to recover, at the TD-MCSCF level, excitation energies which are rather close to the FCI ones as shown in Fig. 2 (a). Near the equilibrium distance the $n{}^1\Sigma_g^+$ excited states ($n = 2, \dots, 5$), as described by the TD-MCSCF model, are dominated by the singly excited configuration $(1\sigma_g)^1(n\sigma_g)^1$. This statement holds at the TD-MC-srLDA level for the first three lowest ${}^1\Sigma_g^+$ excited states, which explains why, in the light of Sec. IV A, the corresponding excitation energies are very close to the TD-HF-srLDA ones, as shown in Fig. 2 (b). On the other hand, the TD-MC-srLDA $5{}^1\Sigma_g^+$ state is dominated by the doubly excited configuration $(1\sigma_u)^2$ already at the equilibrium distance. This is illustrated by the large difference between the TD-HF-srLDA and TD-MC-srLDA excitation energies at 1.4 a.u. Note that, at the TD-MCSCF level, the doubly excited character of the $5{}^1\Sigma_g^+$ state appears only at 2 a.u., when the slope of the potential curve suddenly changes. Upon bond stretching, the avoided crossing of the TD-MC-srLDA $5{}^1\Sigma_g^+$ and $4{}^1\Sigma_g^+$ states occurs around 2 a.u. The latter gains a doubly excited character which explains the deviation of its excitation energy from the TD-HF-srLDA one. Note that regular TD-LDA as well as TD-HF-srLDA methods

completely miss the $5^1\Sigma_g^+$ state for stretched geometries. Returning to the $4^1\Sigma_g^+$ state, the TD-MC-srLDA exhibits an avoided crossing with the $3^1\Sigma_g^+$ state around 2.5 a.u. The latter is then dominated by the doubly excited configuration $(1\sigma_u)^2$. As a consequence the TD-HF-srLDA and TD-MC-srLDA $3^1\Sigma_g^+$ excitation energies differ significantly when stretching the bond beyond 2.5 a.u. Another avoided crossing occurs, at 3 a.u. in the TD-MC-srLDA model, between the $3^1\Sigma_g^+$ and $2^1\Sigma_g^+$ states. While regular TD-LDA as well as TD-HF-srLDA keep on describing the lowest $^1\Sigma_g^+$ excited state as singly excited for large bond distances, the TD-MC-srLDA method is able to catch the double excitation $(1\sigma_g)^2 \rightarrow (1\sigma_u)^2$, which is included in the active space. For analysis purposes, TD-MC-srLDA excitation energies have been computed when $\mu = 0$ (see Fig. 3). As shown in the Appendix, even though the ground-state MC-srLDA wave function reduces to the regular KS-LDA determinant, the TD-MC-srLDA ($\mu = 0$) method recovers not only the TD-LDA spectrum but also the double excitation $(1\sigma_g)^2 \rightarrow (1\sigma_u)^2$ whose excitation energy is found to be twice the KS orbital energy difference $2(\varepsilon_{\sigma_u} - \varepsilon_{\sigma_g})$. This explains the crossings in Fig. 3. As pointed out in Sec. IID, the double excitation should in principle be disregarded since it does not correspond to a pole of the density. Still, it is interesting to note that the TD-MC-srLDA ($\mu = 0.4$) avoided crossings shown in Fig. 2 (b) originate from this unphysical solution. Let us stress that, for $\mu = 0.4$, the double excitation described within TD-MC-srLDA is, on the other hand, physical. This is ensured by non-zero orbital rotation coefficients (not shown) in the corresponding linear response vector as well as the multi-configurational character of the ground-state MC-srLDA wave function in stretched geometries. Finally, as in Sec. IV A, we again conclude that the inaccuracy of the TD-MC-srLDA ($\mu=0.4$) method is essentially due to the approximate short-range potential and kernel used.

C. Singlet excited states of the beryllium atom

Singlet excitation energies of the beryllium atom have been computed at the TD-MC-srDFT level, using the srPBEgws functional and the $2s2p$ active space, when varying the μ parameter. Results are shown in Figs. 4 (a) and 4 (b). Comparison is made with the linear response TD-CCSD results which are used as reference. Let us first mention that, in the $\mu = 0$ limit of the TD-MC-srPBEgws model, standard TD-PBE excitation energies are recovered. Interestingly the 1^1D state, which corresponds to the double excitation

$(2s)^2 \rightarrow (2p)^2$ and which is absent in the standard TD-PBE spectrum, is also described at the TD-MC-srPBEgws level even when $\mu = 0$. In this particular case, the excitation energy actually equals twice the KS-PBE orbital energy difference $2(\varepsilon_{2p} - \varepsilon_{2s})$. As shown in the Appendix, this is due to the fact that the double excitation is included in the active space and can, therefore, be treated explicitly. In this case, the excitation energy turns out to be equal to the TD-CCSD one. Nevertheless, when μ is strictly equal to zero, this double excitation is unphysical as mentioned in Sec. II D. For non-zero μ values, even small ones, this is not the case anymore since the ground-state MC-srPBEgws wave function is multi-configurational and orbital rotations appear in the linear response vector. Let us mention that, at the TD-MC-srLDA level, we obtained a 1^1D excitation energy of 7.17 eV when $\mu = 0.1$ which corresponds to an absolute error of 0.02 eV. In the TD-DMFT-srLDA ($\mu = 0.1$) method of Pernal [23], the absolute error is much larger (2 eV). (We note that Pernal used a different srLDA functional than we used, namely the one by Paziani *et al.* [60], but we do not expect this to be important for the absolute error.) As pointed out by the author this error might be due to the approximate density-matrix functional used for describing the long-range interaction while, in the TD-MC-srDFT model, the latter is explicitly treated at the MCSCF level. When increasing the μ parameter, the TD-MC-srPBEgws 1^1D excitation energy deviates slightly from the TD-CCSD one, by less than 0.15 eV. Note that the TD-MC-srLDA 1^1D excitation energy was found to be equal to 6.96 eV for $\mu = 0.4$ a.u., which corresponds to an absolute deviation of 0.23 eV. The absolute error obtained at the TD-DMFT-srLDA ($\mu = 0.4$) level by Pernal [23] is much larger (3.38 eV), which we again attribute to the approximate density-matrix functional used for modeling the long-range interaction. The other excitation energies are all underestimated at the regular TD-PBE level. Those can be improved significantly when μ becomes larger than 0.2 a.u. The difference between the TD-HF-srPBEgws and TD-MC-srPBEgws excitation energies increases then with μ since electron correlation is transferred from the short-range DFT part to the long-range MCSCF part of the linear response equations. We note that, for most of the states, TD-MC-srPBEgws can perform better than TD-HF-srPBEgws and the regular TD-MCSCF model, which is recovered in the $\mu \rightarrow +\infty$ limit, but different μ values should then be used. As extensively discussed in Ref. [24] it is more appealing, in order to have a general method, to set the μ parameter to a fixed value, using prescriptions for an optimal treatment of correlation for example, and improve the accuracy of the short-range

functionals. Work is in progress in this direction.

D. ferrocene

A major objective stimulating the development of the TD-MC-srDFT model is to pave the way for an efficient computational tool of predictive power that allows us to study excitation spectra of large, complex molecular systems where for example local and charge-transfer (CT) excitations often co-occur. As an illustrative example we computed the low-lying singlet excitation spectrum of ferrocene for which experimental solution data [61, 62] as well as ample theoretical *ab initio* gas-phase reference values [49, 50, 63–65] are available.

A ground-state HF calculation for ferrocene with the Cp-rings in D_{5h} symmetric configuration around the d^6 Fe(II) center yields the following energetic order of iron-centered high-lying occupied (non-bonding) and anti-bonding LUMO d -orbitals:

$$a'_1(d_{z^2}; d_\sigma) \approx e'_2(d_{x^2-y^2}, d_{xy}; d_\delta) \ll e''_1(d_{xz}, d_{yz}; d_\pi).$$

In addition, we find as highest occupied MOs (doubly degenerate HOMO orbitals) predominantly Cp-centered, bonding π -orbitals. In summary, the valence configuration reads as: $(a'_1)^2 (e'_2)^4 (e''_1)^4 (e''_1)^0$.

Based on this ground state occupation we can expect a manifold of three doubly-degenerate (E''_1, E''_2, E''_1) singlet metal-centered valence transitions which will be examined in Section IV D 1 as well as ligand-to-metal CT excitations in the ultra-violet visible spectrum to be discussed in Section IV D 2. In particular in the latter case it will be interesting to examine whether our new TD-MC-srDFT scheme can improve TD-DFT/CAM-B3LYP. In TD-DFT/CAM-B3LYP both long- and short-range correlations are treated in DFT whereas in TD-MC-srDFT the long-range correlation is handled with MCSCF.

All experimental data available to us is recorded in solution, and a fair comparison of the computed data would thus require to account for solvent effects which was beyond the scope of the present investigation. Work in that direction is currently in progress [66]. Hence, we *assume* that the metal-centered transitions are rather insensitive to solvent effects due to their local character whereas the CT transitions are more likely to be sensitive to solvation effects because of potentially strong ligand-solvent interactions.

Before embarking on details of the excited state spectrum compiled in Table I we com-

mence with a brief examination of the geometry dependence of our data. For this purpose, we performed TD-DFT/CAM-B3LYP calculations with ferrocene (*i*) in a staggered conformation with D_{5d} symmetry (for geometrical data see Table S2 in the Supplementary Material [45]) and (*ii*) in a second eclipsed conformation with geometrical parameters taken from experiment [67–69] which was used by Ishimura *et al.* [49] in their symmetry adapted cluster-configuration interaction (SACCI) excited state calculations (see Table S3 in the Supplementary Material [45]). We find that the lowest-lying singlet excited states are hardly affected by adapting to a staggered conformation. The *d-d* excitation energies are lowered to a minor degree to 2.29 eV, 2.62 eV and 3.43 eV with a maximum deviation of $\Delta_{max} = -0.04$ eV from the reference TD-DFT/CAM-B3LYP values (D_{5h} -symmetric configuration) listed in Table I. Larger deviations with $\Delta_{max} = -0.10$ eV are observed for the second eclipsed configuration of ferrocene where the *d-d* excitation energies read as 2.23 eV, 2.56 eV and 3.37 eV. The latter should be taken into account when comparing our final results with the SACCI data given in Table I.

1. Metal-centered *d-d* transitions

Table I comprises in the upper part the spin-allowed singlet *d-d* transition energies. For further analysis we summarize in Table II the relative energy gaps Δ_1 and Δ_2 , respectively which are determined from the excitation energy differences between E_2'' and the lower E_1'' state and the higher-lying singlet *d-d* transition E_1'' and E_2'' .

Turning first to the transition energies computed at the TD-HF level of theory reveals strikingly the importance of accounting for electron correlation. We find deviations from experiment by more than 1.8 eV for the lower E_1'' and E_2'' states. The comparatively close match of the second E_1'' transition of 3.39 eV with the experimental reference of 3.82 eV is fortuitous. The TD-MCSCF approach in contrast allows to recover a significant part of the dynamic electron correlation in the excited states since all *d*-orbitals involved in the low-lying *d-d* transitions are included in the active CAS(10,10) space. This indeed leads to overall, greatly improved absolute excitation energies. The third excited state E_1'' , however, is located at only 3.15 eV giving rise to a too close gap $\Delta_2 = 0.19$ eV and in addition, Δ_1 hardly changes compared to TD-HF.

The excited state data derived from regular TD-DFT calculations listed in Tables I and

They follow general tendencies that can be summarized as follows. Introducing a fraction of full-range exact HF exchange like in B3LYP (20 %) and CAM-B3LYP (19 %) compared to the LDA and PBE functionals correlates with decreasing excitation energies in contrast to increasing energetic gaps $\Delta_{1,2}$. In general, this results in a closer agreement with experiment using hybrid functionals. Hence, we may order the accuracy of the functionals studied here as CAM-B3LYP \approx B3LYP $>$ PBE $>$ LDA. As one could expect for the rather spatially localized $d-d$ transitions the hybrid B3LYP functional performs similarly well compared to the more sophisticated CAM-B3LYP functional which includes an additional 46 % of long-range HF exchange. Let us now consider the excitation energies and their energetic separations Δ_1 and Δ_2 computed by means of TD-HF-srDFT. Using 100% of long-range HF exchange, irrespective of the choice of srLDA or srPBE functionals, reduces the transition energies and enlarges their relative gaps Δ_1 and Δ_2 in comparison to the regular TD-DFT/LDA and TD-DFT/PBE data, respectively. This is not only in line with the findings for (CAM-)B3LYP relative to LDA and PBE but results also in a good agreement of TD-HF-srDFT with the hybrid functionals. Clearly, $\mu = 0.4$ a.u. is large enough to introduce a non-negligible part of HF exchange, since long-range effects do not appear to be significant in the $d-d$ excitations. The fact that TD-MC-srPBEgws and TD-HF-srPBEgws results are not equal elucidates that a non-negligible part of the two-electron interaction is indeed assigned to the long-range interaction and thus treated by the MCSCF approach within the CAS(10,10) active space. In accordance with Fromager *et al.* [24], total energy differences on the order of 10^{-2} a.u. between the ground-state HF-srPBEgws and MC-srPBEgws wave functions, respectively, corroborate our conclusion. In passing, we note that our TD-MC-srPBEgws data are in very good agreement with experiment with respect to both excitation energies and the relative energetic spacings $\Delta_{1,2}$ of the three lowest electronic singlet $d-d$ transitions. The largest deviation to experiment is for the third excited state (located at 3.82 eV) where all approaches studied here yield too low transition energies except for SACCI which, not taking into account further geometry effects (*vide supra*), slightly overshoots by +0.21 eV. In summary, based on the experimental references, our new TD-MC-srPBEgws method shows significantly enhanced performance compared to the multi-reference wave function SACCI approach which yields only a moderate agreement with experiment both with respect to transition energies and their energetic separation $\Delta_{1,2}$. Moreover, TD-MC-srPBEgws provides a valuable alternative to the otherwise well-performing hybrid (CAM-

)B3LYP functionals as well as the model potential LB94 which was explored in the recent work by Scuppa and co-workers [50].

2. *Ligand \rightarrow Metal charge-transfer excitations*

We report in the lower part of Table I CT excitation energies computed at the TD-HF, TD-DFT level employing LDA, GGA, B3LYP and CAM-B3LYP functionals along with our TD-HF/MC-srDFT results. The experimental data refers to the maximum peak positions in the measured absorption spectrum of ferrocene. It is readily seen that the TD-HF CT excitation energies are unacceptably high whereas the TD-DFT/LDA and TD-DFT/PBE transitions are too close to the lower end of the visible spectrum. With the hybrid B3LYP functional, on the other hand, deviations from experiment are reduced to -0.41 and -0.48 eV for the first and second CT transitions, respectively, yielding excitation energies of 5.41 eV and 5.72 eV. This clearly indicates the importance of using an exact exchange energy, or at least a fraction of it, with regard to a more general description of CT states where the extent of exact exchange determines the *partial* correction of the “long-range” self-interaction error intrinsically present for pure LDA and GGA-type functionals. The appropriate combination with a suitable correlation functional then leads to satisfying results as seen here for B3LYP. Bearing this in mind, the superior performance of CAM-B3LYP compared to B3LYP with respect to the ligand-to-metal CT excitations might not be unexpected as CAM-B3LYP comprises in addition to the 19% of full-range HF exchange energy (B3LYP: 20%), 46% of the long-range exact exchange energy. Although only a fraction of long-range HF exchange is used, fortuitous error cancellations in combination with an approximate correlation density-functional may lead to excellent results, where CAM-B3LYP excitation energies at the triple- ζ basis set level nearly coincide with the experimental solution data. Turning to the oscillator strengths, they are too weak in all our calculations, which is probably a combination of basis set effects and the solvent effects on the experiments.

A closer inspection of the CT transitions in Table I further reveals that both TD-DFT/LDA and TD-HF predict the CT transitions in reversed order. This feature remains also in the picture predicted by our TD-MCSCF response calculations where the description of long-range and short-range dynamic correlation within the CAS(10,10) space vastly improves the excitation energies, lowering them to 5.50 eV for the A_2'' and 6.24 eV for the E_1' state while,

at large, their relative gap (in reversed order) enlarges to 0.74 eV compared to 0.38 eV in experiment. The extended active orbital space treated within the SACCI approach, on the other hand, seems to capture most of the important contributions to the CT transitions, thus illustrating the importance of short-range dynamic correlation. Peaks are predicted closely spaced at 6.34 eV and 6.43 eV, respectively, though. Similar conclusions can be drawn for the TD-HF-srDFT model with either the srLDA or srPBEgws functional. The straightforward inclusion of short-range dynamic correlation by means of the srDFT functional, using $\mu = 0.4$ a.u., suffices in this context to recover the correct CT state order from the $\mu \rightarrow +\infty$ pure wave-function-based TD-HF limit. In contrast to the local d - d transitions (see Sec. IV D 1) we observe for the first CT state a large difference between the TD-HF-srDFT and TD-DFT/CAM-B3LYP approaches which we ascribe mainly to different fractions of long-range HF exchange, which amounts to only 65% in CAM-B3LYP, and more importantly, to missing long-range correlation in TD-HF-srDFT. The impact of describing the latter correlation type explicitly, within the MCSCF model, is highlighted by our TD-MC-srPBEgws results. It lowers the first E'_1 transition by 0.35 eV compared to TD-HF-srPBEgws while the second main CT peak is pushed upwards to 7.04 eV, thus overshooting the experimental reference by ≈ 0.8 eV. A detailed analysis shows that the second CT transition is, within both the TD-MCSCF and TD-MC-srPBEgws approaches, fully described by orbital rotations whereas the optically allowed E'_1 transition is largely obtained by configuration rotations. However, one cannot make any final conclusions about the quality of the TD-MC-srPBEgws results compared to experiments before the solvent effects have been included in the calculations. Work on this is currently in progress. Computing high-level gas phase CC excitation energies would also be interesting for benchmarking.

To sum up, our new proposed TD-MC-srDFT model has promising potential to accurately describe not only local excitations as shown for example for the d - d transitions in Sec. IV D 1 but also to simultaneously model charge transfer excitations and their corresponding relative oscillator strengths. It exhibits in particular improved performance compared to both TD-DFT based on pure density-functionals and TD-MCSCF. In contrast to the latter approach, the srPBEgws functional combined with a long-range TD-MCSCF treatment is able to describe short-range dynamic correlations and enables to get the two CT states in predicted order. The relative energy difference between the two CT states seems too large, though, when compared to experimental data. This might be due to self-interactions errors induced

by the employed short-range functionals where the formers could be reduced choosing a different separation of short-range exchange and correlation energies. Work is currently in progress in this direction. Moreover, the inclusion of solvation effects by means of a polarizable embedded framework into the TD-MC-srDFT and TD-DFT response approaches [66] of the DALTON2011 program framework will facilitate future comparison to experimental works recorded in solution. Finally, we note that the TD-MC-srDFT scheme seems to be a viable alternative to TD-DFT/CAM-B3LYP where, in the former case, long-range correlation effects are described at the MCSCF level. Further calibration studies focusing particularly on such a direct comparison are being prepared.

V. CONCLUSIONS

The extension of multi-determinant range-separated DFT to the time-dependent regime has been investigated. Following Vignale [25, 26], an exact variational formulation was obtained. Various approximate schemes can then be formulated, depending on the choice of the post-HF method that is used for describing the long-range interaction, and the choice of the exchange-correlation functional used for treating the short-range interaction. In this work, the combination of long-range MCSCF with short-range adiabatic LDA and GGA was considered. The corresponding linear response scheme, referred to as TD-MC-srDFT, was then derived within Floquet theory. Numerical results obtained for the singlet excited states of the stretched H_2 molecule and Be show that TD-MC-srDFT can, in contrast to regular TD-DFT, describe double excitations even though the adiabatic approximation is used for the short-range exchange-correlation density-functional contributions. This is made possible by the MCSCF-type parametrization of the wave function where, in addition to orbital rotations, configuration rotations inside the active space can be treated explicitly. For the commonly used $\mu = 0.4$ range-separation parameter value, excitation energies are, in most cases, much better described with TD-MC-srDFT than regular TD-DFT. Huge improvements are also observed, when comparing with the TD-DMFT-srLDA results of Pernal [23], in the description of the 1^1D doubly-excited state of Be and the $1^1\Sigma_u^+$ state of the stretched H_2 molecule. Still, in the latter case, excitation energies are significantly underestimated. The error is due to the approximate short-range LDA and GGA potential and kernel that are used. Increasing μ improves on the accuracy but then some part of the

short-range electron correlation is transferred from DFT to the MCSCF. This is of course not appealing, in terms of computational cost, for larger scale calculations. As an alternative, a different decomposition of the short-range exchange and correlation energies [58–60] could be used while keeping the μ parameter set to 0.4 a.u. Work is currently in progress in this direction. The accuracy of the TD-MC-srDFT approach using a short-range GGA functional was further examined for the low-lying singlet excited states of the d^6 metallocene ferrocene. Excitation energies as well as energetic state separations are in overall good agreement with experiment for both valence and charge-transfer excitations apart from a single outlier. TD-MC-srDFT generally outperforms traditional wave-function and TD-DFT approaches with exception of TD-DFT/CAM-B3LYP that yields comparable results with a better performance for the charge-transfer states. The latter functional was specifically designed to remedy known shortcomings of TD-DFT [18] for this excitation class, though. Extensive works with the overall aim to shed further light on weaknesses and strengths of our proposed TD-MC-srDFT approach with respect to TD-DFT/CAM-B3LYP are therefore in progress. Particular focus is in this context laid on model excited-state charge-transfer compounds such as peptides, carotenoides [70] and transition metal complexes [71].

Acknowledgments

S.K. acknowledges the Danish Natural Science Research Council for an individual post-doctoral grant (10-082944). Computing resources were provided by the Danish Center for Scientific Computing (DCSC) at the University of Southern Denmark in Odense. E.F. thanks ANR (contract DYQUMA) as well as Kenneth Ruud, Radovan Bast, Andreas Thorvaldsen and Julien Toulouse for fruitful discussions on response theory.

APPENDIX: TWO-STATE TD-MC-srDFT MODEL IN THE $\mu = 0$ LIMIT

Let us consider a minimal active space consisting of two Slater determinants $|a^2\rangle$ and $|b^2\rangle$ representing doubly-occupied ϕ_a and ϕ_b orbitals, respectively. The former determinant corresponds to the ground-state KS determinant which is recovered at the MC-srDFT level in the $\mu = 0$ limit (see Sec. II A). For simplicity, orbital rotations are not considered in the following. According to Eqs. (7) and (8) in Ref. [41], the long-range Hessian $E_0^{[2]\mu}$ and the

metric $S^{[2]\mu}$ introduced in Eqs. (38) and (39) become, when $\mu = 0$,

$$E_0^{[2]0} = \begin{bmatrix} A^0 & B^0 \\ B^{0*} & A^{0*} \end{bmatrix}, \quad S^{[2]0} = \begin{bmatrix} \Sigma^0 & \Delta^0 \\ -\Delta^{0*} & -\Sigma^{0*} \end{bmatrix}, \quad (\text{A1})$$

where

$$\begin{aligned} A^0 &= \begin{bmatrix} \langle a^2 | [\hat{R}_{a^2}, [\hat{H}^{\text{KS}}, \hat{R}_{a^2}^\dagger]] | a^2 \rangle & \langle a^2 | [\hat{R}_{a^2}, [\hat{H}^{\text{KS}}, \hat{R}_{b^2}^\dagger]] | a^2 \rangle \\ \langle a^2 | [\hat{R}_{b^2}, [\hat{H}^{\text{KS}}, \hat{R}_{a^2}^\dagger]] | a^2 \rangle & \langle a^2 | [\hat{R}_{b^2}, [\hat{H}^{\text{KS}}, \hat{R}_{b^2}^\dagger]] | a^2 \rangle \end{bmatrix}, \\ B^0 &= \begin{bmatrix} \langle a^2 | [\hat{R}_{a^2}, [\hat{H}^{\text{KS}}, \hat{R}_{a^2}]] | a^2 \rangle & \langle a^2 | [\hat{R}_{a^2}, [\hat{H}^{\text{KS}}, \hat{R}_{b^2}]] | a^2 \rangle \\ \langle a^2 | [\hat{R}_{b^2}, [\hat{H}^{\text{KS}}, \hat{R}_{a^2}]] | a^2 \rangle & \langle a^2 | [\hat{R}_{b^2}, [\hat{H}^{\text{KS}}, \hat{R}_{b^2}]] | a^2 \rangle \end{bmatrix}, \\ \Sigma^0 &= \begin{bmatrix} \langle a^2 | [\hat{R}_{a^2}, \hat{R}_{a^2}^\dagger] | a^2 \rangle & \langle a^2 | [\hat{R}_{a^2}, \hat{R}_{b^2}^\dagger] | a^2 \rangle \\ \langle a^2 | [\hat{R}_{b^2}, \hat{R}_{a^2}^\dagger] | a^2 \rangle & \langle a^2 | [\hat{R}_{b^2}, \hat{R}_{b^2}^\dagger] | a^2 \rangle \end{bmatrix}, \\ \Delta^0 &= \begin{bmatrix} \langle a^2 | [\hat{R}_{a^2}, \hat{R}_{a^2}] | a^2 \rangle & \langle a^2 | [\hat{R}_{a^2}, \hat{R}_{b^2}] | a^2 \rangle \\ \langle a^2 | [\hat{R}_{b^2}, \hat{R}_{a^2}] | a^2 \rangle & \langle a^2 | [\hat{R}_{b^2}, \hat{R}_{b^2}] | a^2 \rangle \end{bmatrix}, \end{aligned} \quad (\text{A2})$$

$$\hat{R}_{a^2}^\dagger = |a^2\rangle\langle a^2|, \quad \hat{R}_{b^2}^\dagger = |b^2\rangle\langle a^2|,$$

and $\hat{H}^{\text{KS}} = \hat{T} + \hat{V}_{\text{ne}} + \hat{V}_{\text{Hxc}}[n_{a^2}]$ denotes the non-interacting KS Hamiltonian. Since $\hat{H}^{\text{KS}}|a^2\rangle = 2\varepsilon_a|a^2\rangle$ and $\hat{H}^{\text{KS}}|b^2\rangle = 2\varepsilon_b|b^2\rangle$, the matrices in Eq. (A2) can be simplified as follows

$$\begin{aligned} A^0 &= \begin{bmatrix} 0 & 0 \\ 0 & 2(\varepsilon_b - \varepsilon_a) \end{bmatrix}, \\ B^0 &= \Delta^0 = 0, \end{aligned} \quad (\text{A3})$$

$$\Sigma^0 = \begin{bmatrix} 0 & 0 \\ 0 & 1 \end{bmatrix}.$$

In addition, the gradient density vector defined in Eq. (37) becomes in the $\mu = 0$ limit:

$$n^{[1]0}(\mathbf{r}) = \begin{bmatrix} 0 \\ \langle b^2 | \hat{n}(\mathbf{r}) | a^2 \rangle \\ 0 \\ -\langle a^2 | \hat{n}(\mathbf{r}) | b^2 \rangle \end{bmatrix} = 0, \quad (\text{A4})$$

since $|a^2\rangle$ and $|b^2\rangle$ differ by a double excitation. As a result the kernel contribution to the Hessian defined in Eq. (40) equals zero when $\mu = 0$ so that the total Hessian is simply $E_0^{[2]0}$. We thus conclude from Eqs. (A1) and (A3) that the double excitation $a^2 \rightarrow b^2$ is described within the TD-MC-srDFT model in the $\mu = 0$ limit and the corresponding excitation energy is twice the KS orbital energy difference $2(\varepsilon_b - \varepsilon_a)$. In this respect, the TD-MC-srDFT model does not reduce to standard TD-DFT, as the TD-HF-srDFT model does, in the $\mu = 0$ limit. Still, in this example, the double excitation is a pole of the TD-MC-srDFT wave function but not of the density since the linear response contribution to the density $n^{[1]0\dagger}(\mathbf{r})X(\omega)$ always equals zero, according to Eq. (A4). From this point of view, the double excitation obtained at the TD-MC-srDFT ($\mu = 0$) level is unphysical.

-
- [1] E. Runge and E. K. U. Gross, *Phys. Rev. Lett.* **52**, 997 (1984).
- [2] M. Casida, in *Recent Advances in Density Functional Methods*, edited by D. P. Chong (World Scientific, Singapore, 1995).
- [3] A. Savin, *Recent Developments and Applications of Modern Density Functional Theory* (Elsevier, Amsterdam, 1996), p. 327.
- [4] O. A. Vydrov and G. E. Scuseria, *J. Chem. Phys.* **125**, 234109 (2006).
- [5] J. W. Song, T. Hirose, T. Tsuneda, and K. Hirao, *J. Chem. Phys.* **126**, 154105 (2007).
- [6] M. J. G. Peach, P. Benfield, T. Helgaker, and D. J. Tozer, *J. Chem. Phys.* **128**, 044118 (2008).
- [7] M. A. Rohrdanz, K. M. Martins, and J. M. Herbert, *J. Chem. Phys.* **130**, 054112 (2009).
- [8] P. Elliott, S. Goldson, C. Canahui, and N. T. Maitra, *Chem. Phys.* **391**, 110 (2011).
- [9] N. T. Maitra, F. Zhang, R. J. Cave, and K. Burke, *J. Chem. Phys.* **120**, 5932 (2004).
- [10] J. Neugebauer, E. J. Baerends, and M. Nooijen, *J. Chem. Phys.* **121**, 6155 (2004).
- [11] K. Burke, *J. Chem. Phys.* **136**, 150901 (2012).
- [12] N. T. Maitra, K. Burke, and C. Woodward, *Phys. Rev. Lett.* **89**, 023002 (2002).
- [13] Y.-H. Kim and A. Görling, *Phys. Rev. Lett.* **89**, 096402 (2002).
- [14] D. Hofmann, T. Körzdörfer, and S. Kümmel, *Phys. Rev. Lett.* **108**, 146401 (2012).
- [15] G. Malliaras and R. Friend, *Phys. Today* **58**, 53 (2005).
- [16] M. Grätzel, *Inorg. Chem.* **44**, 6841 (2005).
- [17] H. Iikura, T. Tsuneda, T. Yanai, and K. Hirao, *J. Chem. Phys.* **115**, 3540 (2001).
- [18] T. Yanai, D. P. Tew, and N. C. Handy, *Chem. Phys. Lett.* **393**, 51 (2004).
- [19] O. A. Vydrov, J. Heyd, A. V. Krukau, and G. E. Scuseria, *J. Chem. Phys.* **125**, 074106 (2006).
- [20] R. Baer, E. Livshits, and U. Salzner, *Annu. Rev. Phys. Chem.* **61**, 85 (2010).
- [21] M. J. G. Peach, P. Benfield, T. Helgaker, and D. J. Tozer, *J. Chem. Phys.* **128**, 044118 (2008).
- [22] T. Stein, L. Kronik, and R. Baer, *J. Am. Chem. Soc.* **131**, 2818 (2009).
- [23] K. Pernal, *J. Chem. Phys.* **136**, 184105 (2012).
- [24] E. Fromager, J. Toulouse, and H. J. Aa. Jensen, *J. Chem. Phys.* **126**, 074111 (2007).
- [25] G. Vignale, *Phys. Rev. A* **77**, 062511 (2008).
- [26] G. Vignale, *Phys. Rev. A* **83**, 046501 (2011).
- [27] J. Toulouse and A. Savin, *J. Mol. Struct. (Theochem)* **762**, 147 (2006).

- [28] J. Toulouse, F. Colonna, and A. Savin, *Phys. Rev. A* **70**, 062505 (2004).
- [29] J. K. Pedersen, Ph.D. thesis, University of Southern Denmark (2004).
- [30] J. G. Ángyán, I. C. Gerber, A. Savin, and J. Toulouse, *Phys. Rev. A* **72**, 012510 (2005).
- [31] J. Toulouse, I. C. Gerber, G. Jansen, A. Savin, and J. G. Ángyán, *Phys. Rev. Lett.* **102**, 096404 (2009).
- [32] B. G. Janesko, T. M. Henderson, and G. E. Scuseria, *J. Chem. Phys.* **130**, 081105 (2009).
- [33] E. Goll, H. J. Werner, and H. Stoll, *Phys. Chem. Chem. Phys.* **7**, 3917 (2005).
- [34] E. Fromager, R. Cimiraglia, and H. J. Aa. Jensen, *Phys. Rev. A* **81**, 024502 (2010).
- [35] A. M. Teale, S. Coriani, and T. Helgaker, *J. Chem. Phys.* **133**, 164112 (2010).
- [36] J. Olsen and P. Jørgensen, *J. Chem. Phys.* **82**, 3235 (1985).
- [37] O. Christiansen, P. Jørgensen, and C. Hättig, *Int. J. Quantum Chem.* **68**, 1 (1998).
- [38] P. Salek, O. Vahtras, T. Helgaker, and H. Ågren, *J. Chem. Phys.* **117**, 9630 (2002).
- [39] P. Salek, T. Helgaker, and T. Saue, *Chem. Phys.* **311**, 187 (2005).
- [40] T. Saue and H. J. Aa. Jensen, *J. Chem. Phys.* **118**, 522 (2003).
- [41] P. Jørgensen, H. J. Aa. Jensen, and J. Olsen, *J. Chem. Phys.* **89**, 3654 (1988).
- [42] *Dalton2011*, an *ab initio* electronic structure program. See <http://daltonprogram.org/> (2011).
- [43] J. Toulouse, A. Savin, and H. J. Flad, *Int. J. Quantum Chem.* **100**, 1047 (2004).
- [44] T. H. Dunning, *J. Chem. Phys.* **90**, 1007 (1989).
- [45] See Supplementary Material Document No. xxx for bond distances and angles corresponding to the eclipsed and staggered conformer structure of ferrocene.
- [46] S. Coriani, A. Haaland, T. Helgaker, and P. Jørgensen, *Comp. Phys. Comm.* **7**, 245 (2006).
- [47] H. Koch, P. Jørgensen, and T. Helgaker, *J. Chem. Phys.* **104**, 9528 (1996).
- [48] K. Pierloot, B. J. Persson, and B. O. Roos, *J. Chem. Phys.* **99**, 3465 (1995).
- [49] K. Ishimura, M. Hada, and H. Nakatsuji, *J. Chem. Phys.* **117**, 6533 (2002).
- [50] S. Scuppa, L. Orian, D. Dini, S. Santi, and M. Meneghetti, *J. Phys. Chem. A* **113**, 9286 (2009).
- [51] T. H. Dunning Jr., *J. Chem. Phys.* **90**, 1007 (1989).
- [52] N. B. Balabanov and K. Peterson, *J. Chem. Phys.* **123**, 064107 (2005).
- [53] S. H. Vosko, L. Wilk, and M. Nusair, *Can. J. Phys.* **58**, 1200 (1980).
- [54] J. P. Perdew, K. Burke, and M. Ernzerhof, *Phys. Rev. Lett.* **77** (1996).
- [55] A. D. Becke, *J. Chem. Phys.* **98**, 5648 (1993).

- [56] E. Fromager, F. Réal, P. Wåhlin, U. Wahlgren, and H. J. Aa. Jensen, *J. Chem. Phys.* **131**, 054107 (2009).
- [57] K. J. H. Giesbertz, O. V. Gritsenko, and E. J. Baerends, *J. Chem. Phys.* **136**, 094104 (2012).
- [58] J. Toulouse, P. Gori-Giorgi, and A. Savin, *Theor. Chem. Acc.* **114**, 305 (2005).
- [59] P. Gori-Giorgi and A. Savin, *Int. J. Quantum Chem.* **109**, 1950 (2009).
- [60] S. Pazziani, S. Moroni, P. Gori-Giorgi, and G. B. Bachelet, *Phys. Rev. B* **73**, 155111 (2006).
- [61] A. T. Armstrong, F. Smith, E. Elder, and S. P. McGlynn, *J. Chem. Phys.* **46**, 4321 (1967).
- [62] H. B. Gray, Y. S. Sohn, and N. Hendrickson, *J. Am. Chem. Soc.* **93**, 3603 (1971).
- [63] Y. L. Li, L. Han, Y. Mei, and J. Z. Zhang, *Chem. Phys. Lett.* **482**, 217 (2009).
- [64] P. Boulet, H. Chermette, C. Daul, F. Gilardoni, F. Rogemond, J. Weber, and G. Zuber, *J. Phys. Chem. A* **105**, 885 (2001).
- [65] A. Rosa, G. Ricciardi, O. Gritsenko, and E. J. Baerends, *Structure and Bonding* **112**, 49 (2004).
- [66] E. D. Hedegaard, H. J. Aa. Jensen, , and J. Kongsted, *J. Chem. Phys.* (2013), work in progress.
- [67] R. K. Bohn and A. Haaland, *J. Organomet. Chem.* **5**, 2653 (1968).
- [68] A. Haaland and J. E. Nilsson, *Acta Chem. Scand.* **22**, 2653 (1968).
- [69] A. Haaland, J. Lusztyk, D. P. Novak, J. Brunvoll, and K. B. Starowieyski, *J. Chem. Soc. Chem. Commun.* pp. 54–55 (1974).
- [70] E. D. Hedegaard, F. Heiden, E. Fromager, H. J. Aa. Jensen, J. Kongsted, and S. Knecht, *J. Chem. Theory Comput.* (2013), work in progress.
- [71] S. Knecht, E. Fromager, and H. J. Aa. Jensen, *J. Chem. Phys. Communications* (2013), work in progress.

FIGURE CAPTIONS

Figure 1: First (black), second (red), third (green) and fourth (blue) $^1\Sigma_u^+$ excitation energies in H_2 along the bond breaking coordinate calculated with (a) standard TD-MCSCF and TD-LDA methods (b) TD-HF-srLDA and TD-MC-srLDA schemes. Comparison is made with FCI results. Each type of line corresponds to a given method. The μ parameter was set to 0.4 a.u. The minimal active space $1\sigma_g 1\sigma_u$ was used. Basis set is aug-cc-pVQZ.

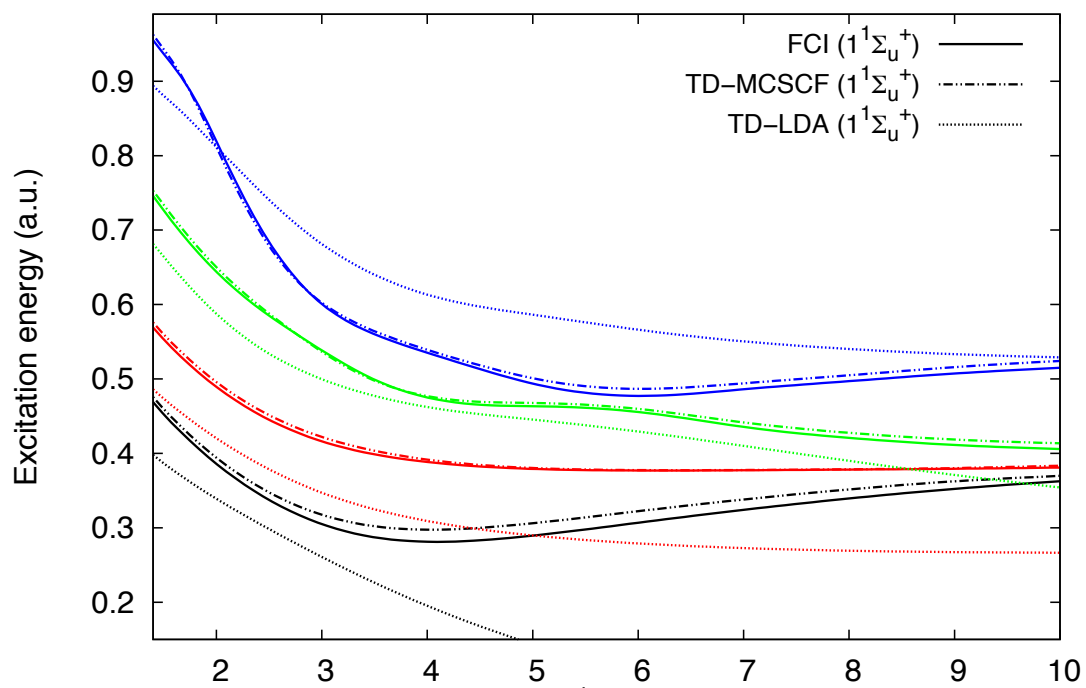
Figure 2: First (black), second (red), third (green) and fourth (blue) $^1\Sigma_g^+$ excitation energies in H_2 along the bond breaking coordinate calculated with (a) standard TD-MCSCF and TD-LDA methods (b) TD-HF-srLDA and TD-MC-srLDA schemes. Comparison is made with FCI results. Each type of line corresponds to a given method. The μ parameter was set to 0.4 a.u. The minimal active space $1\sigma_g 1\sigma_u$ was used. Basis set is aug-cc-pVQZ.

Figure 3: First (black), second (red), third (green) and fourth (blue) $^1\Sigma_g^+$ excitation energies in H_2 along the bond breaking coordinate obtained with the TD-MC-srLDA method, setting $\mu = 0$, and compared to standard TD-LDA results. For analysis purposes, twice the $1\sigma_u$ and $1\sigma_g$ KS-LDA orbital energy difference is also plotted. Each type of line or point corresponds to a given method. The minimal active space $1\sigma_g 1\sigma_u$ was used. Basis set is aug-cc-pVQZ.

Figure 4: Excitation energies obtained in Be when varying μ at the TD-HF-srPBEgws and TD-MC-srPBEgws levels for (a) the 1^1P (black), 2^1S (red), 1^1D (blue) and 2^1D (purple) singlet states (b) the 2^1P (grey), 3^1P (cyan) and 3^1S (green) singlet states. Comparison is made with TD-CCSD results. Each type of line corresponds to a given method. Twice the KS-PBE orbital energy difference $2(\varepsilon_{2p} - \varepsilon_{2s})$ is also plotted for analysis purposes. The minimal active space $2s2p$ was used. Basis set is aug-cc-pVQZ.

FIG. 1: Fromager et al, Journal of Chemical Physics

(a) $\text{H}_2 [n^1\Sigma_u^+, n=1-4]$



(b) $\text{H}_2 [n^1\Sigma_u^+, n=1-4]$

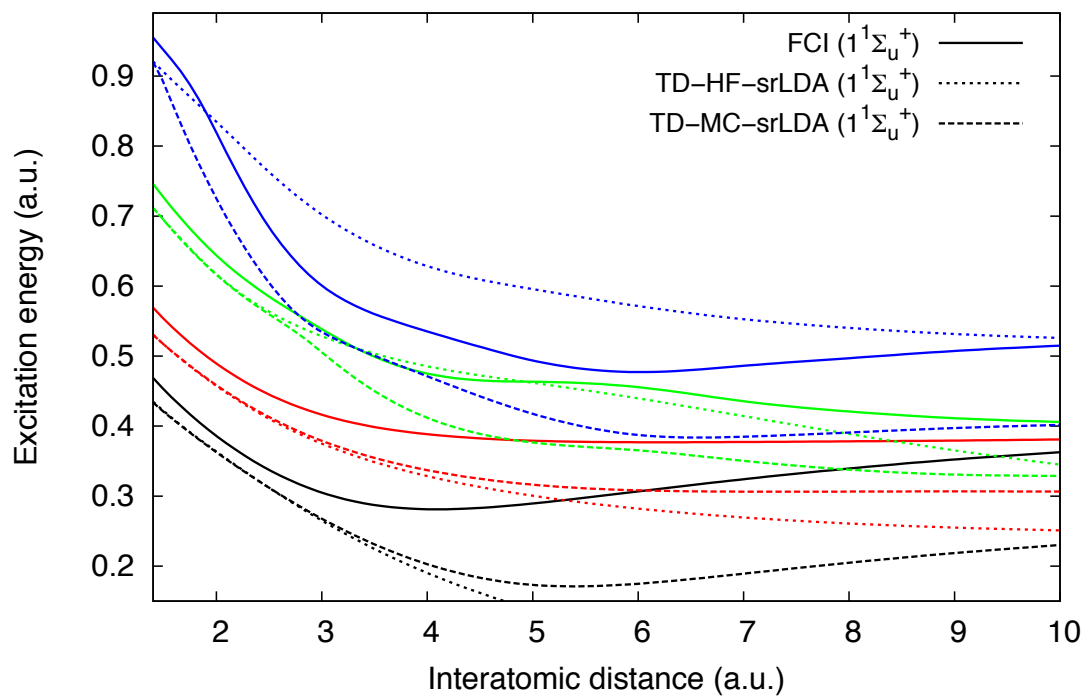


FIG. 2: Fromager et al, Journal of Chemical Physics

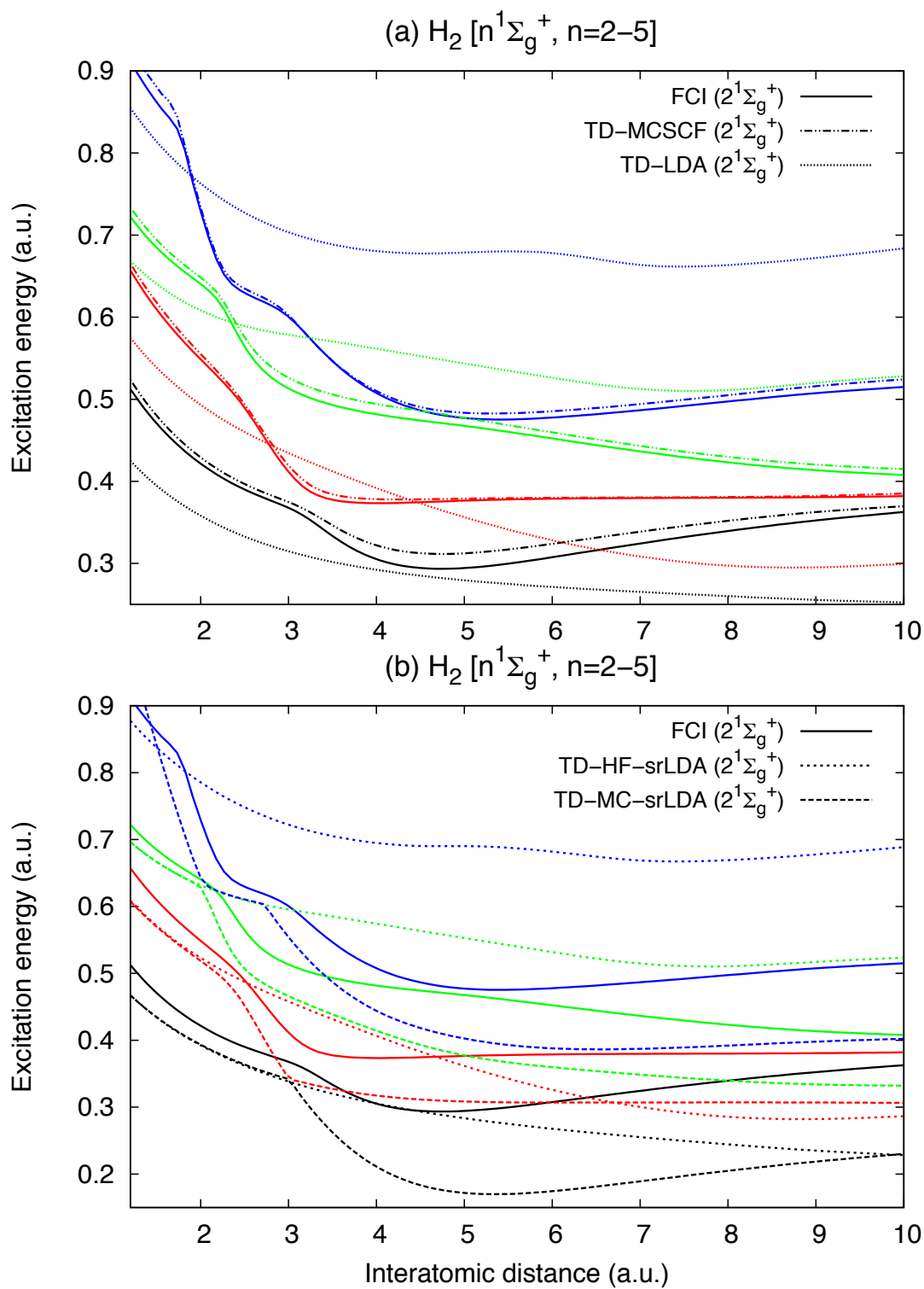


FIG. 3: Fromager et al, Journal of Chemical Physics

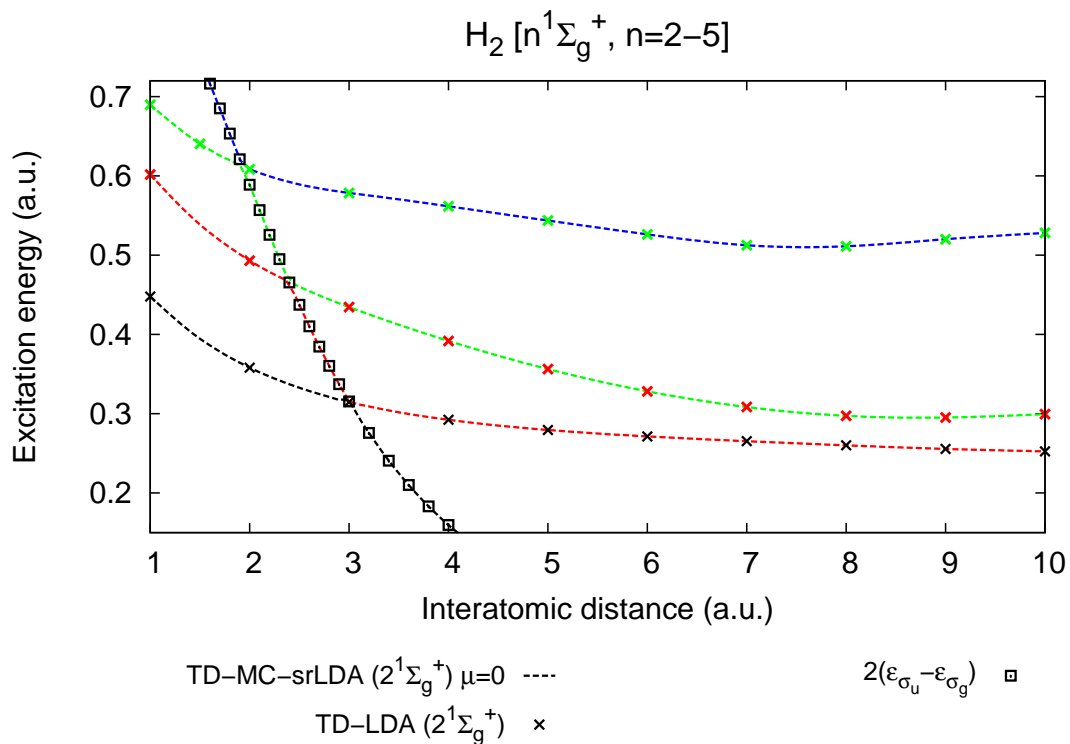


FIG. 4: Fromager et al, Journal of Chemical Physics

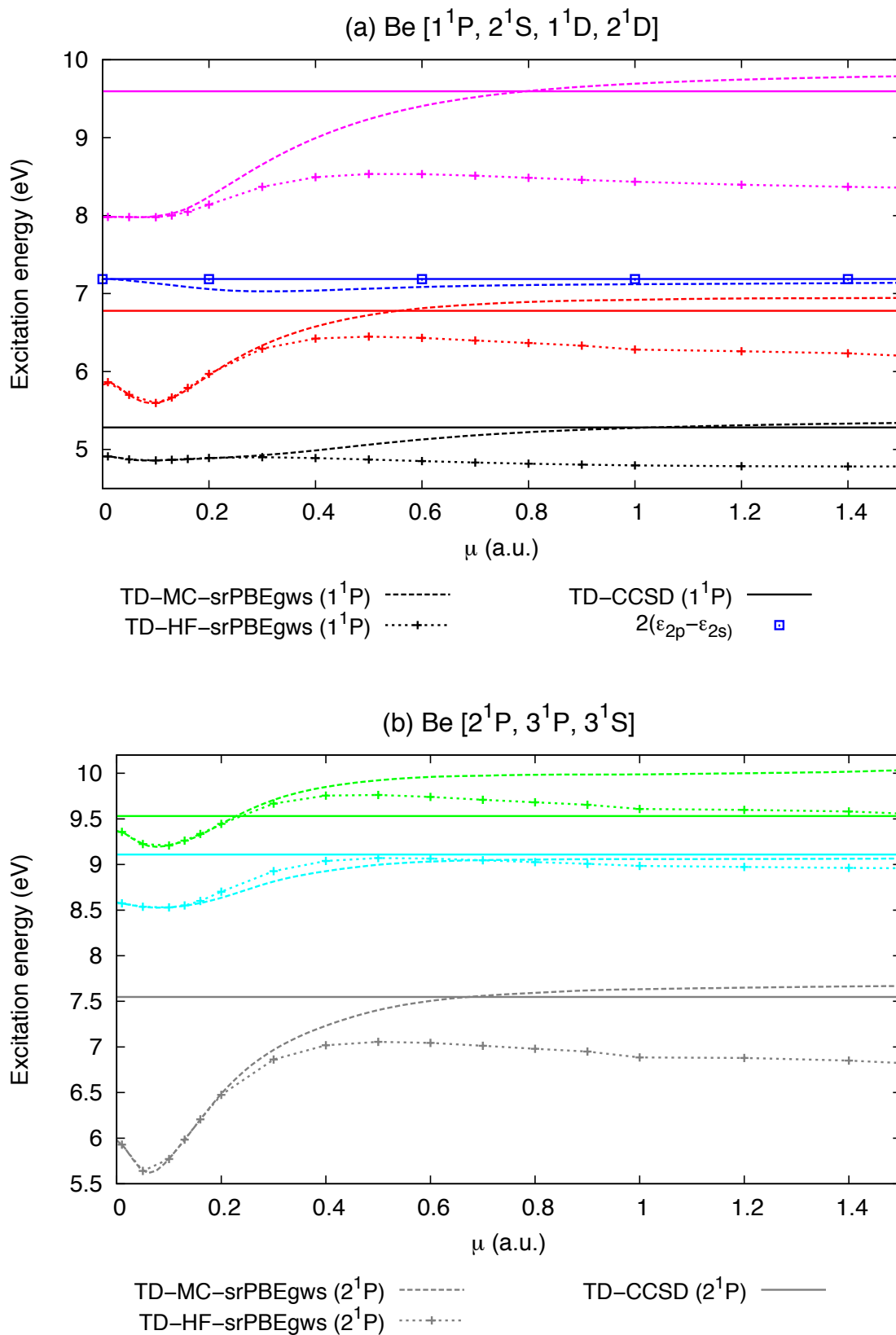


TABLE CAPTIONS

Table I: Key spin-allowed singlet Fe $d-d$ and lowest optically active singlet transition energies (eV) in ferrocene. Oscillator strength f are reported in the row below the charge-transfer state excitation energies for selected, exemplary cases. The abbreviation "TD-" has been omitted for compactness in the table header.

Table II: Energy gaps (in eV) between the lowest three spin-allowed singlet Fe $d-d$ transition energies in ferrocene obtained from TD-MC-srDFT calculations, and compared with other *ab initio* and experimental data. Δ_1 refers to the energetic difference between the lower E_1'' and E_2'' states while Δ_2 quantifies the difference in transition energies between the upper E_1'' and E_2'' states, respectively. The abbreviation "TD-" has been omitted for compactness in the table header.

TABLE I: Fromager et al, Journal of Chemical Physics

State	HF	MCSCF	SACCI ^a	LDA	PBE	LB94 ^b	B3LYP	B3LYP	CAM-	HF-	HF-	MC-	Experiment ^d
									srLDA	srPBE ^c	srPBE ^c		
<i>d-d excitations</i>													
E ₁ ^{''}	0.92	2.82	2.11	2.94	2.90	2.81	2.43	2.33	2.45	2.42	2.59	2.70	2.70
E ₂ ^{''}	1.09	2.96	2.27	2.99	3.03	2.91	2.70	2.65	2.74	2.79	2.88	2.98	2.98
E ₁ ^{''}	3.39	3.15	4.03	3.52	3.60	3.44	3.48	3.45	3.29	3.41	3.50	3.82	3.82
<i>charge-transfer excitations</i>													
E ₁ [']	8.49	6.24	6.34	5.13	5.09	n/a	5.41	5.85	6.28	6.24	5.89	5.82 ^e	5.82 ^e
<i>f</i>	-	0.040	-	-	0.013	-	-	0.018	-	0.024	0.024	0.105	0.105
A ₂ ^{''}	8.12	5.50	6.43	4.89	5.46	n/a	5.72	6.25	6.34	6.39	7.04	6.20 ^f	6.20 ^f
<i>f</i>	-	0.188	-	-	0.002	-	-	0.107	-	0.149	0.171	0.730	0.730

^a Ref. 49, ^b Ref. 50, ^c srPBEgws, ^d Ref. 62, ^e value from Ref. 61, ^f Ref. 61: 6.31 eV (*f*: 0.691).

TABLE II: Fromager et al, Journal of Chemical Physics

Energy gap	HF MCSCF	SACCI ^a	LDA PBE	LB94 ^b	B3LYP	B3LYP	CAM-	HF-	HF-	MC-	Experiment ^d	
								srLDA	srPBE ^c	srPBE ^c		
Δ_1	0.17	0.14	0.16	0.05	0.13	0.10	0.27	0.32	0.29	0.37	0.29	0.28
Δ_2	2.30	0.19	1.76	0.53	0.57	0.53	0.78	0.80	0.55	0.62	0.62	0.84

^a Ref. 49, ^b Ref. 50, ^c srPBEgws, ^d Ref. 62.